Microfluidics and Nanofluidics

www.springer.com/journal/10404

Impact factor = 2.489

Accepted May 3rd 2021

SIMULATION OF THE ONSET OF CONVECTION IN A POROUS MEDIUM LAYER SATURATED BY A COUPLE STRESS NANOFLUID

J.C. Umavathi[1*] and **O. Anwar Bég[2]**

*[1]Department of Mathematics, Gulbarga University, Gulbarga-585 106, Karnataka, **INDIA**.*

*[2]Professor of Engineering Science & Director Multi-Physical Engineering Sciences Group (MPESG), Department of Aeronautical/Mechanical Engineering, School of Science, Engineering and Environment (SEE), University of Salford, Manchester, M5 4WT, **UK**.*

****Corresponding author- email: drumavathi@rediffmail.com***

ABSTRACT

Linear and nonlinear stability analyses for the onset of time-dependent convection in a horizontal layer of a porous medium saturated by a couple-stress non-Newtonian nanofluid, intercalated between two thermally insulated plates, are presented. Brinkman and Maxwell-Garnett formulations are adopted for nanoscale effects. A modified Darcy formulation that includes the time derivative term is used for the momentum equation. The nanofluid is assumed to be dilute and this enables the porous medium to be treated as a weakly heterogeneous medium with variation of thermal conductivity and viscosity, in the vertical direction. The general transport equations are solved with a Galerkin-type weighted residuals method. A perturbation method is deployed for the *linear* stability analysis and a Runge–Kutta–Gill (RKG) quadrature scheme for the *nonlinear* analysis. The critical Rayleigh number, wave numbers for the stationary and oscillatory modes and frequency of oscillations are obtained analytically using linear theory and the non-linear analysis is executed with minimal representation of the truncated Fourier series involving only two terms. The effect of various parameters on the stationary and oscillatory convection behavior is visualized. The effect of couple stress parameter on the stationary and oscillatory convections is also shown graphically. It is found that the couple stress parameter has a stabilizing effect on both the stationary and oscillatory convections. Transient Nusselt number and Sherwood number exhibit an oscillatory nature when time is small. However, at very large values of time both Nusselt number and Sherwood number values approach their steady state values. The study is relevant to the dynamics of biopolymers in solution in microfluidic devices and rheological nanoparticle methods in petroleum recovery.

KEYWORDS: *Non-Newtonian nanofluid; Stokes' couple stress model; porous medium; natural convection; horizontal layer; thermal conductivity; viscosity variation; Brinkman model, Maxwell-Garnetts model; Fourier series; Galerkin method; RKG quadrature.*

NOMENCLATURE

C_P	Couple-stress parameter, $\dfrac{\mu_C}{\mu_{eff}\, H^2}$
D_B	Brownian diffusion coefficient (m^2/s)
D_T	Thermophoretic diffusion coefficient (m^2/s)
H	Dimensional layer depth (m)
k	Thermal conductivity of the nanofluid (W/m K)
k_m	Effective thermal conductivity of the porous medium saturated by the nanofluid (W/m K)
K	Permeability of saturated porous medium (m^2)
Ln	Lewis number
N_A	Modified diffusivity ratio
N_B	Modified particle-density increment
p^*	Pressure (Pa)
p	Dimensionless pressure, $\left(p^* K\right)/\left(\mu\alpha_f\right)$
Ra_T	Thermal Rayleigh - Darcy number
Rm	Basic-density Rayleigh number
Rn	Solutal (concentration) Rayleigh number
t^*	Time (s)
t	Dimensionless time, $\left(t^*\alpha_f\right)/H^2$
T^*	Nanofluid temperature (K)
T	Dimensionless temperature, $\dfrac{T^* - T_c^*}{T_h^* - T_c^*}$
T_c^*	Temperature at the upper wall (K)
T_h^*	Temperature at the lower wall (K)
(u,v,w)	Dimensionless Darcy velocity components $\left(u^*, v^*, w^*\right)H/\alpha_m$ (m/s)
$\boldsymbol{v}$	Nanofluid velocity vector (m/s)

Va	Vadász number
(x, y, z)	Dimensionless Cartesian coordinate $(x^*, y^*, z^*)/H$; [z is the vertically upward Coordinate]
(x^*, y^*, z^*)	Cartesian coordinates

Greek symbols

α_f	Thermal diffusivity of the fluid, (m/s^2)
β	Thermal volumetric coefficient (K^{-1})
γ_a	Non-dimensional acceleration
ν	Viscosity variation parameter
ε	Porosity
η	Conductivity variation parameter
μ	Viscosity of the fluid (kg/ms)
ρ	Fluid density (kg/m^3)
ρ_p	Nanoparticle mass density (kg/m^3)
σ	Thermal capacity ratio
ϕ^*	Nanoparticle volume fraction
ϕ	Relative nanoparticle volume fraction, $\frac{\phi^* - \phi_0^*}{\phi_1^* - \phi_0^*}$

Superscripts

*	Dimensional variable
'	Perturbed variable
St	Stationary
Osc	Oscillatory

Subscripts

b	Basic solution
f	Fluid
p	Particle

1. INTRODUCTION

Non-Newtonian fluids are finding increasing applications in modern microfluidics. They feature in droplet generation in microfluidic T-junctions [1], miniaturizing assays passive flow control [2] and particle micro-separation techniques [3]. In these applications, minute volumes of fluids can be accommodated via a versatile platform at small length scales. Engineers are able to design in regimes with very high deformation rates at moderate to vanishing Reynolds numbers. Lu *et al.* [4] have shown that *non-Newtonian fluids* are much more effective in for example inertial microfluidics where larger volumes of fluid samples are required at a high throughput. Newtonian fluids are less efficient since they do not possess the elastic lift features of non-Newtonian fluids for manipulation of particles of smaller size and over an extensive range of flow rates. Viscoelasticity for example has been fruitfully utilized in porous media microfluidics [5], cell and particle trapping in biomicrofluidics [6] and shear-thinning droplet formation in microfluidic junctions [7].

In recent years *nano-scale systems* have also emerged as a major thrust in advanced technological applications (aerospace, medical, energy). Prior to the use of nano-sized particles of metals and metal oxides, engineers experimented with millimeter- or micrometer-sized particles in fluids Although these particles improved the thermal conductivity of the fluid, they resulted in other problems such as agglomeration, settling, drastic pressure drops, clogging channels and premature wear in channels and other components. Since nanoparticles approach the size of the molecules in the fluid, the nano-sized particles have an advantage over milli- and micro-sized particles. For example, nanoparticles generally do not settle under gravity and this mitigates clogging and wearing of channels, which is particularly important in microfluidics. The suspensions of nanoscale particles (either carbon-based e.g. silicates or metallic e.g. gold, copper, silver etc) in the base fluids are known as nanofluids and were introduced by Choi [8] at Argonne National Energy Labs., USA in the mid-1990s. Due to their potential for high rate of heat exchange incurring either little or no penalty in the pressure drop, nanofluids have attracted enormous interest from researchers and have been exploited in solar energy [9], pharmacodynamics [10], smart coatings [11], nano-lubricants [12], petroleum drilling muds [13] and many other industries [14]. The convective heat transfer characteristics of nanofluids depend on the thermophysical properties of the base fluid and the ultra fine particles, the flow pattern and flow structure, the volume fraction of

the suspended particles and the *dimensions and the shape* of these particles. The utility of any particular nanofluid for a heat transfer application can be established by suitably modeling the convective transport in the nanofluid as noted by Kumar *et al*. [15]. The particles are different from conventional particles (millimeter or micro-scale) in that they stay in suspension in the fluid and no sedimentation occurs. Different concepts have been proposed to predict the effective thermal conductivity of the nanofluids and to explain this enhancement in heat transfer [16]. Nanofluid dynamics involve *four scales*: the *molecular scale, the microscale, the macroscale, and the mega-scale*, and an interaction is known to take place between these scales [17] which manifests in thermal enhancement properties. Important studies in this regard include Zhou and Gao [18], Gao and Zhou [19] and Gao *et al.* [20] in which it has been demonstrated experimentally that the effective thermal conductivity increment may also depend on the shape of nanoparticles. Using Bruggeman's model, Keblinski *et al.* [21] proposed a differential effective medium theory to approximate the effective thermal conductivity of nanofluids with non-spherical solid nanoparticles considering interfacial thermal resistance across the solid particles and the host fluids. They observed that if the shape of nanoparticles deviated greatly from spherical then a high enhancement of effective thermal conductivity was attainable. New mechanisms for the exceptional transport of thermal energy in nanofluids have been suggested by many researchers. Koo and Kleinstreuer [22] observed that the role played by Brownian motion is much more vital than the role played by thermophoretic and osmo-phoretic motions. In conclusion, on the one hand, some investigators surmise that nanoparticle aggregation plays an important role in thermal transport due to their chain shape. However, on the other hand other investigators propose that the *time-dependent* thermal conductivity in the nanofluids manifests in a modification in thermal conductivity due to clustering of nanoparticles with time, as noted by Karthikeyan *et al*. [23].

Although many studies of laminar and turbulent nanofluid flows have been communicated, another area of considerable interest in microfluidics is *thermal stability* or the *onset of convection.* A seminal summary of Newtonian problems has been provided in the monumental treatise of Chandrasekhar [24]. The study of the onset of convection in a porous medium layer is known as the Horton-Rogers-Lapwood (HRL) problem [25]. Straughn [26] investigated the effect of an anisotropic inertia coefficient in Darcian flows, computing the

modification in critical Rayleigh number for the onset of convective motion in a porous layer with thermal and solutal effects using both linear instability theory and an energy method for nonlinear stability. Non-Newtonian characteristics of nanofluids have been confirmed at various volume fractions in many experimental investigations including Anil *et al.* [27] (in heat exchangers where rheology of Fe_2O_3, Al_2O_3 and CuO nanoparticles in aqueous carboxymethyl cellulose (CMC) base fluid was studied) and Hussanan *et al.* [28] (for copper metallic nanoparticles in multiple base fluids). Further corroboration of nanofluid rheology has been provided by Jang *et al.* [28]. Several studies of non-Newtonian nanofluid thermal instability have been communicated. Agarwal and Rana [30] computed both the linear and nonlinear onset of convection in a viscoelastic alumina-ethylene-glycol nanofluid saturated densely packed horizontal rotating porous layer heated from below and cooled from above. They deployed the Oldroyd-B type viscoelastic fluid and Brinkman porous model and assumed local thermal non-equilibrium between three phases (porous matrix, fluid, and nanoparticles) and utilized a one-term Galerkin scheme for linear stability and a truncated Fourier series for nonlinear analysis. Kang *et al.* [31] used a power-law shear-thinning model to study the onset of convection in rheological nanofluids in porous media, noting that the most unstable perturbations are transverse rolls, and both traveling-wave and oscillatory modes may occur. They also observed a prominent modification in critical Rayleigh number with the increasing power-law index and Péclet number. They also showed that lowering the Lewis number may either accelerate or delay the onset of thermal convection, depending on the nanoparticle distribution.

The above studies neglected internal microstructure. In the category of non-Newtonian fluids, *couple stress fluids* have distinct features, such as *polar* effects. In these fluids, introduced by Stokes [32], micro-structures become hydrodynamically significant when the characteristic dimension of the problem is of the same order of magnitude as the size of the micro-structure. Couple stress fluids possess no microstructure at the *kinematic* level and therefore the kinematics of such fluids is *totally* described using the *velocity* field [33]. They are much simpler to simulate than micropolar, simple microfluids and other microstructural liquids e.g. microstretch fluids, which require additional balance equations for rotary gyration, angular momentum etc. An excellent review of couple stress (polar) fluid dynamics has been provided by Cowin [34]. It is further noteworthy that the micro-structure

size is the same as the average pore size and therefore couple stress (polar fluids) are appropriate for transport modelling in porous media. The principal effect of couple stresses is therefore to introduce a *length-dependent effect* which is absent in the classical non-polar fluid dynamics (Navier- Stokes model). Couple stress fluid dynamics has been implemented in an impressive range of studies including squeeze film tribology [35], geological flows [36], rotating magnetic membrane oxygenators in medicine [37], spin bioreactors [38], propulsion [39], lubrication [40], electrokinetic microfluidics [41], materials processing [42] and supercritical coating heat transfer [43]. Thermal instability in couple stress fluids has also garnered some interest in mathematical simulation. Important studies in this regard include Patil and Hiremath [44] who studied natural convection (thermal buoyancy) effects in instability of couple stress fluids in a Darcian permeable regime. Nandal and Mahajn [45] considered heat generation or absorption effects in the onset of couple stress fluid convection. Sunil and Mahajan [46] analysed the global nonlinear stability threshold for convection in a couple-stress fluid using linear instability theory, noting that the couple-stress fluid is thermally more stable than the Newtonian fluid. Kumar *et al.* [47] studied rotational body force effects on the onset of thermosolutal convection in couple stress fluids. Gaikwad *et al.* [48] considered the influence of cross diffusion on couple stress thermal linear and nonlinear instability. The thermal stability of an electrically conducting couple-stress fluid-saturated porous layer in the presence of magnetic field was investigated by Sharma and Thakur [49], in which it was observed that increasing couple stress effect postpones the onset of stationary convection. Sunil *et al.* [50] studied the stability of a superposed couple stress fluids in porous medium with magnetic effect, deriving a sufficient condition for the non-existence of over-stability. The onset of convection in a couple stress fluid saturated porous layer in the presence of rotation and magnetic field was studied by Sharma and Sharma [51]. Malashetty *et al.* [52] analysed the hydrodynamic linear stability of a couple stress fluid saturated horizontal Darcian porous layer heated from below and cooled from above when the fluid and solid phases are not in local thermal equilibrium. Using asymptotic and exact methods, they showed that the results of the thermal non-equilibrium Darcy model for the Newtonian fluid case may be retrieved in the limit for *vanishing* couple stress parameter. All these studies confirmed the significant influence of couple stresses on convective instability.

In the context of *nanofluid thermal instability simulation*, several approaches are available for simulating nanoscale effects. Buongiorno [53] proposed a two-component model incorporating the effects of Brownian diffusion and the thermophoresis. However, this methodology ignores the influence of volume fraction and cannot be used to simulate different nanoparticles. An alternative approach is to ignore Brownian motion and thermophoresis and instead focus on the effects of *variation of thermal conductivity and viscosity with nanofluid particle fraction*, utilizing expressions obtained with the mathematical theory of mixtures. This approach has been employed by Tiwari and Das [54] and is based on Brinkman and Maxwell-Garnetts formulations which are adopted in the current study in combination with cross-diffusion effects.

Thermal instability in rheological nanofluids in porous media, as noted, is a subject of some relevance to microfluidic systems. The problem of onset of convection in a porous medium layer saturated with Newtonian fluids and non-Newtonian nanofluids has been extensively studied in the literature. However, relatively sparse attention has been given to the study of onset of convection in a porous medium layer saturated with couple stress non-Newtonian fluids with supplementary thermophysical effects. Although couple stress nanofluid dynamics has been reported in other areas e.g. squeezing flows [55] and Sakiadis stretching sheet flows [56], nevertheless it has not been studied in thermal instability in porous media. Therefore, motivated by addressing this area of relevance to rheological microfluidics, in the present article the *onset of thermosolutal convection in a layer of porous medium saturated by a couple stress nanofluid sandwiched between parallel plates with cross diffusion (Soret/Dufour) effects* is analyzed. The impact of couple stress parameter, viscosity variation parameter, conductivity variation parameter together with other governing parameters on the hydrodynamic stability of the regime is investigated rigorously with Galerkin, Shooting quadrature and truncated Fourier series methods. Both linear and weakly non-linear stability analysis are presented. Further the non-linear steady and unsteady stability analysis is studied in terms of Nusselt and Sherwood numbers.

2. MATHEMATICAL THERMOSOLUTAL MODEL

2.1 Conservation equations

A coordinate frame in which the *z*-axis is aligned vertically upwards is employed. A couple-stress fluid saturated horizontal porous layer confined between the planes $z^* = 0$ and $z^* = H$ is examined. Asterisks are used to denote dimensional variables. Each boundary wall is assumed to be a perfect thermal conductor. The physical model is shown in **Fig. 1.** The size of nanoparticles is small relative to pore size of the matrix, nanoparticle topology is spherical and they are suspended in the nanofluid which avoids their agglomeration and deposition on the porous matrix. The couple stress nanofluid is incompressible as is the porous matrix. The nanoparticles and couple stress nanofluid (polymer) are uncharged. Nanoparticles do not adhere to the nanofluid polymer structure. Nanofluid transport is considered in a microchannel system, not a *nanofluidic channel.*

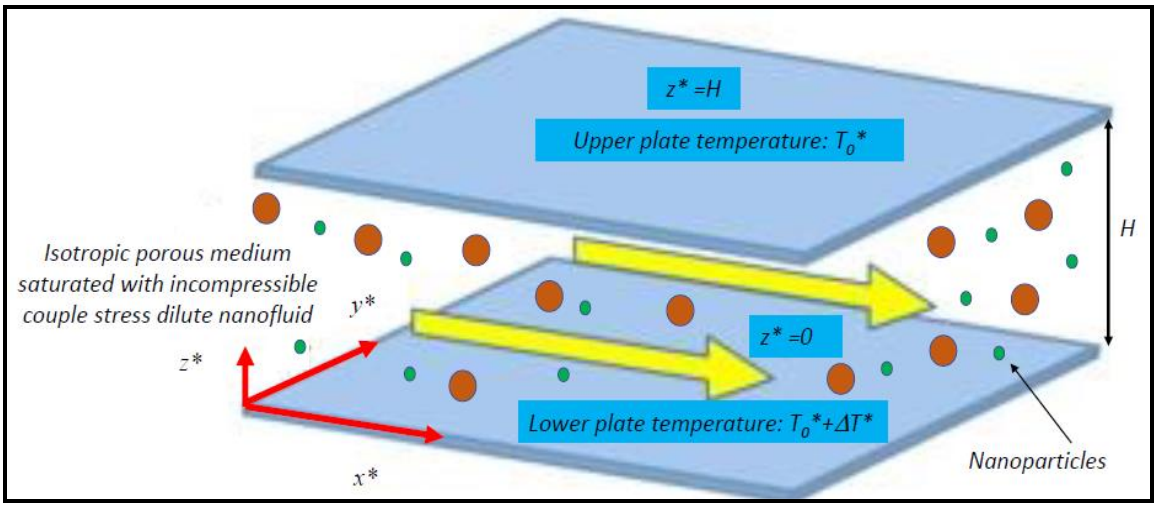

Fig. 1 Geometric model of a nanofluid couple stress layer in a rigid porous medium microfluidic channel

The temperatures at the lower and upper boundary are taken to be $T_0^* + \Delta T^*$ and T^*.The Oberbeck Boussinesq approximation is employed. In the linear stability theory being applied here, the temperature change in the fluid is assumed to be *small* in comparison with T_0^*. The mass conservation (D'Alembert) equation takes the form:

$$\nabla^* . \mathbf{v}_D^* = 0 \tag{1}$$

Here, $\mathbf{v}_D^*$ is the nanofluid Darcy velocity. We write $\mathbf{v}_D^* = \left(u^*, v^*, w^*\right)$.

In the presence of thermophoresis, the conservation equation for the nanoparticles, in the absence of chemical reactions, takes the form:

$$\frac{\partial \phi^*}{\partial t^*} + \frac{1}{\varepsilon}\mathbf{v}_D^*.\nabla\phi^* = \nabla^*.\left[D_B \nabla^*\phi^* + D_T \frac{\nabla^* T^*}{T^*} \right] \tag{2}$$

where ϕ^* is the nanoparticle volume fraction, ε is the medium porosity, T^* is the temperature, D_B is the Brownian diffusion coefficient, and D_T is the thermophoretic diffusion coefficient. Invoking a thermal buoyancy force and adopting the Boussinesq approximation and the Darcy viscous-dominated model for a porous medium, then the modified momentum equation can be written as follows:

$$\frac{\rho}{\varepsilon}\frac{\partial \mathbf{v}_D^*}{\partial t^*} = -\nabla^* p^* - \frac{1}{K}\left(\mu_{eff} - \mu_C\right)\mathbf{v}_{\mathrm{D}}^* + \rho\,\mathrm{g} \tag{3}$$

Here ρ is the overall density of the nanofluid, which we now assume to be given by the following expression:

$$\rho = \phi^*\rho_{\mathrm{p}} + \left(1-\phi^*\right)\rho_0\left[1-\beta_{\mathrm{T}}\left(T^* - T_0^*\right)\right] \tag{4}$$

where ρ_{p} is the particle density, ρ_0 is a reference density for the fluid, and β_{T} is the thermal volumetric expansion. The thermal energy (heat conservation) equation for a nanofluid can be written as

$$\left(\rho c\right)_{\mathrm{m}}\frac{\partial T^*}{\partial t^*} + \left(\rho c\right)_{\mathrm{f}}\mathbf{v}_{\mathrm{D}}^*.\nabla^* T^* = k_{\mathrm{m}}\nabla^{*2}T^* + \varepsilon\left(\rho c\right)_{\mathrm{p}}\left[D_{\mathrm{B}}\nabla^*\phi^*.\nabla T^* + D_{\mathrm{T}}\frac{\nabla T^*.\nabla T^*}{T^*} \right] \tag{5}$$

The conservation of nanoparticle mass (species) requires that:

$$\frac{\partial \phi^*}{\partial t^*} + \frac{1}{\varepsilon}\mathbf{v}_{\mathrm{D}}^*.\nabla^*\phi^* = D_{\mathrm{B}}\nabla^{*2}\phi^* + \frac{D_{\mathrm{T}}}{T_C^*}\nabla^{*2}T^* \tag{6}$$

here c is the fluid specific heat (at constant pressure i.e. isobaric conditions), k_m is the overall thermal conductivity of the porous medium saturated by the nanofluid, and c_p is the specific heat of the material constituting the nanoparticles.

Thus,

$$k_m = \varepsilon k_{eff} + (1-\varepsilon)k_s \tag{7}$$

where ε is the porosity, k_{eff} is the effective conductivity of the nanofluid (fluid plus nanoparticles), and k_s is the conductivity of the solid material forming the matrix of the porous medium.

We now introduce the viscosity and the conductivity dependence on nanoparticle fraction. Following Tiwari and Das [29] we adopt the following formulae, based on a theory of mixtures:

$$\frac{\mu_{eff}}{\mu_f} = \frac{1}{(1-\phi^*)^{2.5}} \tag{8}$$

$$\frac{k_{eff}}{k_f} = \frac{(k_p + 2k_f) - 2\phi^*(k_f - k_p)}{(k_p + 2k_f) + \phi^*(k_f - k_p)} \tag{9}$$

Here k_f and k_p are the thermal conductivities of the fluid and the nanoparticles, respectively.

Eqn (8) is that derived first by Brinkman [57], and Eq. (9) is the *Maxwell-Garnett formula* for a suspension of spherical particles originally presented by Maxwell [58].

In the case where ϕ^* is small compared with unity, we can approximate these formulae by:

$$\frac{\mu_{eff}}{\mu_f} = 1 + 2.5\phi^*, \qquad \frac{k_{eff}}{k_f} = \frac{(k_p + 2k_f) - 2\phi^*(k_f - k_p)}{(k_p + 2k_f) + \phi^*(k_f - k_p)} = 1 + 3\phi^* \frac{(k_p - k_f)}{(k_p + 2k_f)} \tag{10}$$

We assume that the temperature and the volumetric fraction of the nanoparticle are constant on the boundaries (microfluidic channel plates). Thus, the boundary conditions imposed are:

$$w^* = 0,\ T^* = T_0^* + \Delta T^*, \phi^* = \phi_0^* \text{ at } z^* = 0, \qquad w^* = 0,\ T^* = T_0^*, \phi^* = \phi_1^* \text{ at } z^* = H \tag{11}$$

We introduce dimensionless variables as follows:

$$(x, y, z) = (x^*, y^*, z^*)/H,\ t = t^* \alpha_m / \sigma H^2, \quad (u, v, w) = (u^*, v^*, w^*)H/\alpha_m, \quad p = p^* K / \mu_f \alpha_m,$$

$$\phi = \frac{\phi^* - \phi_0^*}{\phi_1^* - \phi_0^*},\ T = \frac{T^* - T_0^*}{\Delta T^*},\ C_P = \frac{\mu_C}{\mu_{eff} H^2} \tag{12}$$

Here C_P is the Stokes couple stress (rheological) parameter and $\alpha_m = \frac{k_m}{(\rho c_p)_f}$, $\sigma = \frac{(\rho c_p)_m}{(\rho c_p)_f}$.

We further define:

$$\tilde{\mu} = \frac{\mu_{eff}}{\mu_f},\ \tilde{k}_p = \frac{k_p}{k_f}, \quad \tilde{k}_s = \frac{k_s}{k_f}, \quad \tilde{k} = \frac{k_m}{k_f} \tag{13}$$

From Eqns. (7), (10) and (13), we have:

$$\tilde{\mu} = 1 + 2.5[\phi_0^* + \phi(\phi_1^* - \phi_0^*)], \quad \tilde{k} = \varepsilon \left\{ 1 + 3[\phi_0^* + \phi(\phi_1^* - \phi_0^*)] \frac{\tilde{k}_p - 1}{\tilde{k}_p + 2} \right\} + (1 - \varepsilon)\tilde{k}_s \tag{14}$$

Then Eqns. (1) and (3) with (4), (5), (2), (11) take the form:

$$\nabla.\mathbf{v} = 0 \tag{15}$$

$$\left(\gamma_a \frac{\partial \mathbf{v}}{\partial t} + \nabla p + Rm\,\hat{e}_z - Ra_T\,\hat{e}_z + Rn\,\phi\,\hat{e}_z\right) + \tilde{\mu}\,\mathbf{v}\left(1 - Cp\nabla^2\right) = 0 \tag{16}$$

$$\frac{\partial T}{\partial t} + \mathbf{v}.\nabla T = \tilde{k}\nabla^2 T + \frac{N_B}{Ln}\nabla\phi.\nabla T + \frac{N_A N_B}{Ln}\nabla T.\nabla T \tag{17}$$

$$\frac{1}{\sigma}\frac{\partial \phi}{\partial t} + \frac{1}{\varepsilon}\mathbf{v}.\nabla\phi = \frac{1}{Ln}\nabla^2\phi + \frac{N_A}{Ln}\nabla^2 T \tag{18}$$

$$w = 0, T = 1, \phi = 0 \quad at \quad z = 0, \qquad w = 0, T = 0, \phi = 0 \quad at \quad z = 1 \tag{19}$$

Here

$$\gamma_a = \frac{\varepsilon}{\sigma Va}, Ln = \frac{\alpha_m}{D_B}, Va = \frac{\varepsilon^2 \,\mathrm{Pr}}{Da},\ \mathrm{Pr} = \frac{\mu_f}{\rho\alpha_m}, Da = \frac{K}{H^2},\ Ra_T = \frac{\rho_0 gK\left(1-\phi_0^*\right)\beta_T H\Delta T^*}{\mu_f \alpha_m},$$

$$Rm = \frac{\left[\rho_p\phi_0^* + \rho_0(1-\phi_0^*)\right]gKH}{\mu_f\alpha_m}, Rn = \frac{(\rho_p - \rho_0)(\phi_1^* - \phi_0^*)gKH}{\mu_f\alpha_m}, N_A = \frac{D_T\Delta T^*}{D_B T_c^*(\phi_1^* - \phi_0^*)},$$

$$N_B = \frac{(\rho c)_p(\phi_1^* - \phi_0^*)}{(\rho c)_f}\ .$$

The parameter γ_a is the non-dimensional acceleration coefficient, Ln is a Lewis number, Va is a Vadász number (a porosity modified Prandtl-Darcy number), Pr is the Prandtl number, Da is the Darcy number and Ra_T is the familiar thermal Rayleigh–Darcy number. The new parameters *Rm* and *Rn* may be regarded as a basic-density Rayleigh number and a concentration (solutal) Rayleigh number, respectively. The parameter N_A is a modified diffusivity ratio and is somewhat similar to the Soret parameter that arises in cross-diffusion (thermo-diffusion) phenomena in solutions, while N_B is a modified particle-density increment.

Eqn. (16) has been linearized by neglecting a term proportional to the product of ϕ and *T*. This assumption is likely to be valid in the case of small temperature gradients in a dilute suspension of nanoparticles.

2.2. Fundamental Solutions

We seek a time-independent quiescent solution of Eqns. (15) – (19) with temperature and nanoparticle volume fraction varying in the *z*-direction only i.e. a solution of the form:

$$\mathbf{v}=0,\ p=p_b(z),\ T=T_b(z),\ \phi=\phi_b(z) \tag{20}$$

Eqns. (16) - (18) reduce to the following coupled ordinary differential equations:

$$0 = -\frac{dp_b}{dz} - Rm + Ra_T T_b - Rn\phi_b \tag{21}$$

$$\tilde{k}\frac{d^2T_b}{dz^2} + \frac{N_B}{Ln}\frac{d\phi_b}{dz}\frac{dT_b}{dz} + \frac{N_A N_B}{Ln}\left(\frac{dT_b}{dz}\right)^2 = 0 \tag{22}$$

$$\frac{d^2\phi_b}{dz^2} + N_A\frac{d^2T_b}{dz^2} = 0 \tag{23}$$

According to Buongiorno [53] this formulation is valid for most dilute nanofluids provided $Ln/\left(\phi_1^* - \phi_0^*\right)$ is large, of the order $10^5 - 10^6$, and since the nanoparticle fraction decrement is typically no smaller than 10^3 this means that Ln is large, of order $10^2 - 10^3$, while N_A is no greater than about 10. Using this approximation, the basic solution emerges as:

$$T_b = 1 - z \text{ and so } \phi_b = z \tag{24}$$

2.3. Perturbation solution

We now superimpose perturbations on the fundamental (basic) solution. We write:

$$\mathbf{v} = \mathbf{v}'\ ,\ p = p_b + p',\ \ T = T_b + T', \phi = \phi_b + \phi' \tag{25}$$

Substitution in Eqns. (13)-(18), and linearization by neglecting products of primed quantities, leads to the following equations by virtue of Eqn. (24):

$$\nabla.\mathbf{v}' = 0 \tag{26}$$

$$\left(\nabla p' + \gamma_a\frac{\partial \mathbf{v}'}{\partial t} - Ra_T T'\hat{e}_z + Rn\phi'\hat{e}_z\right) + \tilde{\mu}\left(1 - Cp\nabla^2\right)\mathbf{v}' = 0 \tag{27}$$

$$\frac{\partial T'}{\partial t} - w' = \tilde{k}\nabla^2 T' + \frac{N_B}{Ln}\left(\frac{\partial T'}{\partial z} - \frac{\partial \phi'}{\partial z}\right) - \frac{2N_A N_B}{Ln}\frac{\partial T'}{\partial z} \tag{28}$$

$$\frac{1}{\sigma}\frac{\partial \phi'}{\partial t} + \frac{1}{\varepsilon}w' = \frac{1}{Ln}\nabla^2\phi' + \frac{N_A}{Ln}\nabla^2 T' \tag{29}$$

$$w' = 0\,,\ T' = 0\,, \phi' = 0 \text{ at } z = 0 \text{ and at } z = 1 \tag{30}$$

It is now possible to approximate the viscosity and thermal conductivity distributions by substituting the basic solution expression for ϕ, namely that given by Eqn. (24), into Eqn. (14). We obtain:

$$\tilde{\mu}(z) = 1 + 2.5\left[\phi_0^* + (\phi_1^* - \phi_0^*)\, z\right],\ \ \tilde{k}(z) = \varepsilon\left\{1 + 3\left[\phi_0^* + \phi\left(\phi_1^* - \phi_0^*\right) z\right]\frac{\tilde{k}_p - 1}{\tilde{k}_p + 2}\right\} + (1-\varepsilon)\,\tilde{k}_s \qquad (31)$$

It will be noted that the parameter Rm is just a measure of the basic static pressure gradient and is not involved in these and subsequent equations. It is important to recognize that the scenario is one where properties are *heterogeneous*. These are now the viscosity and thermal conductivity (rather that the more usual ones, namely permeability *or hydraulic conductivity* and thermal conductivity). Following the methodology of numerous investigators, as reviewed in Nield [59], it is assumed that the heterogeneity is *weak* in the sense that the maximum variation of a property over the domain considered is small compared with the mean value of that property.

The six unknowns $\mathrm{u}', \mathrm{v}', \mathrm{w}', \mathrm{p}', \mathrm{T}', \phi'$ can be reduced to three via operating on Eqn. (27) with $\hat{e}_z$ *curl curl* and using the identity *curl curl* $\equiv$*grad div* $-\nabla^2$ together with Eqn. (26) and the weak heterogeneity approximation. The result (after using Eqn. (31)) emerges as:

$$\left(s\gamma_a + \tilde{\mu}(z) - \tilde{\mu}(z)\, Cp\nabla^2\right)\nabla^2 w' = Ra_T \nabla_H^2 T' - Rn\nabla_H^2 \phi' \qquad (32)$$

Here ∇_H^2 is the two-dimensional Laplacian operator on the horizontal plane.

The differential equations (27), (28), (32) and the boundary conditions (30) constitute a *linear boundary-value problem* that can be solved using the *method of normal modes*. Proceeding with the analysis, we write:

$$\left(w', T', \phi'\right) = \left[W(z), \Theta(z), \Phi(z)\right]\exp\left(st + ilx + imy\right) \qquad (33)$$

The disturbances are expressed in terms of waves with arbitrary amplitude as shown in Eqn. (33). Here s is a constant to be determined and denotes frequency of the waves and in general is a complex quantity $s = s_r + i\, s_i$. Hence $\left[W(z), \Theta(z), \Phi(z)\right] e^{s_r}$ represents the amplitude of the wave $\left[W(z), \Theta(z), \Phi(z)\right] e^{i\,(s_i t + lx + my)}$. Several cases are of interest:

Case1. If $s_r < 0$, then the system is stable for large time otherwise unstable.

Case2. If $s_r = 0$, then two considerations arise for s_i $\left(s_i = 0,\ s_i \neq 0\right)$. $s_r = 0$ is known as marginal stable. The marginal stable curve divides the region into two parts. (a) *stable region* (b) *unstable region*. If $s_i = 0$ along with $s_r = 0$, the state of the system is stationary

and is designated as the *neutral stability state*. If $s_r \neq 0$ along with $s_r = 0$, then the state of the system is *oscillatory with constant amplitude* ω.

If $s_r = 0$ and $s_i = 0$, then it may be inferred that the *principle of exchange of stability* holds. To check whether the system is stable or not for all arbitrary disturbances, (note that it is difficult to consider exhaustively all types of disturbances) we select a few *representative disturbances* from which it is possible to generate all types of disturbances and then study the stability over these few disturbances. This process is called *normal mode analysis* which is represented in Eqn. (33) where l and m are horizontal wave numbers and s is the frequency. The graphs displayed whether the system is *stable or unstable* for the parameters being varied.

Insertion of Eqn. (33) into the differential equations produces the following system:

$$\left(\left(\tilde{\mu}(z)+\gamma_a s\right)-\tilde{\mu}(z)C_P\left(D^2-\alpha^2\right)\right)\left(D^2-\alpha^2\right)W + Ra_T\,\alpha^2\Theta - Rn\,\alpha^2\,\Phi = 0 \tag{34}$$

$$W+\left(\tilde{k}(z)\left(D^2-\alpha^2\right)+\frac{N_B}{Ln}D-\frac{2N_AN_B}{Ln}D-s\right)\Theta-\frac{N_B}{Ln}D\Phi=0 \tag{35}$$

$$\frac{1}{\varepsilon}W-\frac{N_A}{Ln}\left(D^2-\alpha^2\right)\Theta-\left(\frac{1}{Ln}\left(D^2-\alpha^2\right)-\frac{1}{\sigma}s\right)\Phi=0 \tag{36}$$

$$W=0,\ \Theta=0,\ \Phi=0 \quad \text{at} \quad z=0 \text{ and } z=1 \tag{37}$$

where

$$D\equiv\frac{d}{dz} \text{ and } \alpha=(l^2+m^2)^{1/2} \tag{38}$$

Here α is a *dimensionless horizontal wave number*. For neutral stability the real part of *s* is zero. Hence we now write $s=i\omega$, where ω is real and is a dimensionless frequency. Employing a Galerkin-type weighted residuals method, an approximate solution to the system of Eqns. (34)-(37) is sought. We select the following *trial functions* (satisfying the boundary conditions), $W_p, \Theta_p, \Phi_p\,;\, p=1,2,3.....$ Now we may write.

$$\mathrm{W}=\sum_{p=1}^{N}A_pW_p\,,\ \Theta=\sum_{p=1}^{N}B_p\Theta_P\,,\ \Phi=\sum_{p=1}^{N}C_p\Phi_P \tag{39}$$

Substitution into Eqns. (34)– (37), and rendering expressions on the left-hand sides of those equations (the residuals) orthogonal to the trial functions, leads to a system of 3*N* linear

algebraic equations in the $3N$ unknowns A_p, B_p, C_p, p =1, 2, . . . N. The vanishing of the determinant of coefficients produces the *eigenvalue equation* for the system. One can regard Ra_T as the eigenvalue. This enables the determination of the thermal Rayleigh-Darcy number Ra_T in terms of the other parameters. Trial functions satisfying the boundary condition (37) can be chosen as:

$$W_p = \Theta_p = \Phi_p = \sin p\pi z\,;\, p = 1, 2, 3, \ldots \tag{40}$$

The eigenvalue equation is:

$$\det M = 0 \tag{41}$$

where,

$$M = \begin{bmatrix} M_{11} & M_{12} & M_{13} \\ M_{21} & M_{22} & M_{23} \\ M_{31} & M_{32} & M_{33} \end{bmatrix} \tag{42}$$

and, for $i, j = 1, 2, \ldots, N$,

$$\left(M_{11}\right)_{ij} = -\left\langle \left(\tilde{\mu}(z) + \gamma_a s - \tilde{\mu}(z) C_P D^2\right) W_j D^2 W_i \right\rangle + \alpha^2 \left\langle \left(\tilde{\mu}(z) + \gamma_a s - \tilde{\mu}(z) C_P D^2\right) W_j W_i \right\rangle$$

$$\left(M_{12}\right)_{ij} = -Ra_T \alpha^2 \left\langle W_j \Theta_i \right\rangle$$

$$\left(M_{13}\right)_{ij} = Rn\alpha^2 \left\langle W_j \Phi_i \right\rangle$$

$$\left(M_{21}\right)_{ij} = -\left\langle \Theta_j W_i \right\rangle$$

$$\left(M_{22}\right)_{ij} = -\left\langle \tilde{k}(z) \Theta_j D^2 \Theta_i \right\rangle + \alpha^2 \left\langle \tilde{k}(z) \Theta_j \Theta_i \right\rangle + s \left\langle \Theta_j \Theta_i \right\rangle + \left(\frac{2N_A N_B}{Ln} - \frac{N_B}{Ln} \right) \left\langle \Theta_j D \Theta_i \right\rangle$$

$$\left(M_{23}\right)_{ij} = -\frac{N_B}{Ln} \left\langle \Theta_j D \Phi_i \right\rangle$$

$$\left(M_{31}\right)_{ij} = -\frac{1}{\varepsilon} \left\langle \Theta_j W \right\rangle_i$$

$$\left(M_{32}\right)_{ij} = \frac{N_A}{Ln} \left(-\left\langle \Phi_j D^2 \Theta_i \right\rangle + \alpha^2 \left\langle \Phi_j \Theta_i \right\rangle \right)$$

$$\left(M_{33}\right)_{ij} = \frac{1}{Ln} \left(-\left\langle \Phi_j D^2 \Phi_i \right\rangle + \alpha^2 \left\langle \Phi_j \Phi_i \right\rangle \right) + \frac{s}{\sigma} \left\langle \Phi_j \Phi_i \right\rangle$$

Here

$$\left\langle f(z) \right\rangle \equiv \int_0^1 f(z)\, dz. \tag{43}$$

In the present case, where viscosity and thermal conductivity variations are incorporated, the *critical wave number* is unchanged, and the stability boundary becomes:

$$Ra_T = \frac{1}{\left(\frac{J}{Ln}+\frac{s}{\sigma}\right)\alpha^2}\left[J\left(\frac{J}{Ln}+\frac{s}{\sigma}\right)\left(\left(J\,\eta+s\right)\left(\nu+s\,\gamma_a\right)+\nu C_P J\right)-\frac{Rn\,\alpha^2}{\varepsilon}\left(J\,\eta+s\right)-\frac{Rn\,\alpha^2\,N_A}{Ln}J\right] \tag{44}$$

where

$$J = (\pi^2+\alpha^2),\ \ \nu = 1+1.25\left(\phi_1^*+\phi_0^*\right),\ \eta = \varepsilon+(1-\varepsilon)\tilde{k}_s+\frac{3\left(\phi_1^*+\phi_0^*\right)\varepsilon}{2}\left(\frac{\tilde{k}_p-1}{\tilde{k}_p+2}\right) \tag{45}$$

Linear stability analysis using the Galerkin method for nanofluids is well documented in the literature, see, for example, Kuznetsov and Nield [60, 61] (2010a, b). The detailed explanation and methodology for the Galerkin method is given in the book by Finlayson [62]. Further in this paper we consider only *free-free boundary conditions* and the remaining two possible conditions such as *rigid-rigid* and *free-rigid conditions* are not analyzed.

The expression for Ra_T and corresponding minimum value of Raleigh number is computed. ***Case 1:*** When the value of Rayleigh number is less than the value of the minimum Rayleigh number, disturbances with the wave number α will be stable. ***Case 2:*** When the value of Rayleigh number is equal to the minimum value of the Rayleigh number, then the disturbances will become marginally stable. ***Case 3:*** When the value of Rayleigh number exceeds the minimum value of the Rayleigh number, the disturbances will be unstable.

To understand the onset of convection the following logic is applied: if the Rayleigh number is increased by increasing the governing parameters, then this implies that the onset of convection is *delayed* which helps to *stabilize* the system. On the other hand, if Rayleigh number is decreased by increasing these parameters, then the onset of convection is earlier and the system is *unstable*. The concept of onset of convection is also elucidated in great detail in the classical monograph of Chandrasekhar [24].

We observe that when there is no thermal conductivity variation (that is $\eta = 1$, as when $\tilde{k}_s = 1$ and $\tilde{k}_p = 1$) the effect of viscosity variation is to *increase the critical Rayleigh number*

by a factor ν. The additional effect of thermal conductivity variation η is expressed by equation (45). When $\tilde{k}_s = 1$, the maximum value of η is $2.5\left(\phi_1^* + \phi_0^*\right)$ which is attained when $\varepsilon = 1$ and $\tilde{k}_p \to \infty$.

It is pertinent to note that the factor ν comes from the mean value of $\tilde{\mu}(z)$ over the range [0, 1] and the factor η is the *mean value* of $\tilde{k}(z)$ over the same range. This implies that when evaluating the critical Rayleigh number, it is a good approximation to base that number on the *mean values* of the viscosity and conductivity which are based in turn on the fundamental solution for the nanofluid fraction.

3. LINEAR STABILITY ANALYSIS

3.1 Stationary Mode

For satisfaction of the validity of *principle of exchange of stabilities* (i.e., *steady case*), we have $s = 0$ $\left(i.e., s = s_r + is_i = s_r = s_i = 0\right)$ at the margin of stability. For a first approximation we take $N = 1$. Then the Rayleigh number at which the *marginally stable steady mode* exists becomes:

$$Ra_T^{St} = \frac{\left(\pi^2 + \alpha^2\right)^2 \nu\,\eta}{\alpha^2} + \frac{\left(\pi^2 + \alpha^2\right)^3 \nu\, C_P}{\alpha^2} - Rn\left(N_A + \frac{Ln\,\eta}{\varepsilon}\right) \tag{46}$$

In the absence of variation of viscosity and thermal conductivity parameters $\left(\nu = 1, \eta = 1\right)$, the *stationary Rayleigh number* given by Eq. (46) reduces to:

$$Ra_T^{St} = \frac{\left(\pi^2 + \alpha^2\right)^2}{\alpha^2} + \frac{\left(\pi^2 + \alpha^2\right)^3 C_P}{\alpha^2} - Rn\left(N_A + \frac{Ln}{\varepsilon}\right) \tag{47}$$

The minimum value of the Rayleigh number Ra_T^{St} occurs at the critical wave number $\alpha = \alpha_c$ where $\alpha_c{}^2 = x$ satisfies the equation $2C_P x^2 + \left(1 + C_P\pi^2\right)x - \left(1 + C_P\pi^2\right)\pi^2 = 0$. In the absence of nanoparticles and couple stress fluid effects (vanishing C_P), the stationary Rayleigh number Eq. (47) Reduces to $Ra_T^{St} = \frac{\left(\pi^2 + \alpha^2\right)^2}{\alpha^2}$ with the critical value being $Ra_T^{St} = 4\pi^2 =$

39.48 and with $\alpha_C = \pi = 3.14$, which concurs with the classical Newtonian results obtained by Horton and Rogers [51] and Lapwood [9].

3.2 Oscillatory Mode

We now set $s = i\omega$, where $\omega = \mathrm{Im}(\omega)(\omega_r = 0)$ in Eqn. (44) and clear the complex quantities from the denominator, to obtain:

$$Ra_T = \Delta_1 + i\,\omega\,\Delta_2 \tag{48}$$

For the onset of oscillatory convection, $\Delta_2 = 0$ $(\omega_i \neq 0)$ and this gives a dispersion relation of the form (on dropping the subscript *i*):

$$b_1\left(\omega^2\right)^2 + b_2\left(\omega^2\right) + b_3 = 0 \tag{49}$$

Now Eqn. (48) with $\Delta_2 = 0$ yields:

$$Ra_T{}^{Osc} = a_0\left(a_1 + \omega^2 a_2\right) \tag{50}$$

where b_1, b_2 and b_3 and a_0, a_1 and a_2 and Δ_1 and Δ_2 are lengthy algebraic expressions which are omitted for brevity.

The *oscillatory neutral solutions* can be extracted from Eqn. (50). The process is as follows: Determine the number of positive solutions of Eqn. (49). If there are none, then no oscillatory instability is possible. If there are two, then the minimum (over a^2) of Eqn. (50) with ω^2 given by Eqn. (49) gives the *oscillatory neutral Rayleigh number*. Since Eqn. (49) is quadratic in ω^2, it can generate in excess of one positive value of ω^2 for fixed values of the parameters *Rn, Ln,* N_A, σ, γ_a, ν, η, C_P. However, the present numerical solution of Eqn. (49) for the range of parameters considered here gives only one positive value of ω^2 indicating that there exists *only one oscillatory neutral solution*. The analytical expression for oscillatory Rayleigh number given by Eqn. (50) is *minimized* with respect to the wave number numerically, after substituting for ω^2 (> 0) from Eqn. (49), for various values of the thermophysical parameters in order to elucidate their effects on the onset of oscillatory convection.

4. NONLINEAR STABILITY ANALYSIS

In order to explore how the cross-diffusion coefficient terms influence the nonlinear development of onset of convection in porous layer saturated with nanofluid, it is necessary to solve the full nonlinear Eqn. (15)-(18). However, initially we consider the early stages of nonlinear convection, when the *basic structure of the convective rolls is still determined by the behavior of the linearized solution*. In the neighborhood of the stability boundary, we develop the nonlinear analysis in which the amplitudes are no longer small but finite. For simplicity, we consider the case of two-dimensional rolls, assuming all physical quantities to be independent of *y*. Eliminating the pressure and introducing the stream function we obtain:

$$\left(\nu + s\gamma_a\right)\nabla^2\Psi + \nu C_P\nabla^4\Psi + Ra_T\frac{\partial T}{\partial x} - Rn\frac{\partial S}{\partial x} = 0 \tag{51}$$

$$\frac{\partial T}{\partial t} + \frac{\partial \Psi}{\partial x} = \eta\nabla^2 T + \frac{\partial\left(\Psi, T\right)}{\partial\left(x, z\right)} \tag{52}$$

$$\frac{1}{\sigma}\frac{\partial S}{\partial T} + \frac{1}{\varepsilon}\frac{\partial \Psi}{\partial x} = \frac{1}{Ln}\nabla^2 S + \frac{N_A}{Ln}\nabla^2 T + \frac{1}{\varepsilon}\frac{\partial(\Psi, S)}{\partial(x, z)} \tag{53}$$

We solve Eqns. (43)-(45) subjecting them to *stress-free, isothermal, iso-nano-concentration boundary conditions*:

$$\psi = \frac{\partial^2\psi}{\partial z^2} = T = S = 0 \text{ at } z = 0, 1 \tag{54}$$

To perform a *local non-linear stability analysis*, the following Fourier expressions are deployed:

$$\psi = \sum_{n=1}^{\infty}\sum_{m=1}^{\infty} A_{mn}\left(t\right)\sin\left(m\alpha x\right)\sin\left(n\pi z\right)$$

$$T = \sum_{n=1}^{\infty}\sum_{m=1}^{\infty} B_{mn}\left(t\right)\cos\left(m\alpha x\right)\sin\left(n\pi z\right)$$

$$S = \sum_{n=1}^{\infty}\sum_{m=1}^{\infty} C_{mn}\left(t\right)\cos\left(m\alpha x\right)\sin\left(n\pi z\right) \tag{55a, b, c}$$

Further, we take the modes (1, 1) for the stream function, and (0, 2) and (1, 1) respectively for temperature and nanoparticle concentration, leading to:

$$\psi = A_{11}(t)\sin(\alpha x)\sin(\pi z)$$

$$T = B_{11}(t)\cos(\alpha x)\sin(\pi z) + B_{02}(t)\sin(2\pi z)$$
$$S = C_{11}(t)\cos(\alpha x)\sin(\pi z) + C_{02}(t)\sin(2\pi z) \qquad (56)$$

Here the amplitudes $A_{11}(t), B_{11}(t), B_{02}(t), C_{11}(t)$ and $C_{02}(t)$ are functions of time and are to be determined from the dynamics of the system.

The first effect of non-linearity is to distort the temperature and concentration fields through the interaction of ψ, T and ψ, S. The distortion of these fields will correspond to a change in the horizontal mean, i.e., a component of the form $\sin(2\pi z)$ will be generated. It is obvious that ψ is minimally represented, since it is the simplest possible form for satisfying the boundary condition; it is also the form of ψ for the stability problem. The amplitude $A_{11}(t)$ is (generally) a function of time and must be determined. The term $B_{11}(t)\cos(\alpha x)\sin(\pi z)$ is also a minimal representation for θ and is included since it must balance the stream function term in the heat transport equation. The term $B_{02}(t)\sin(2\pi z)$ represents the minimal representation for the distortion of the mean temperature field. The reason for the value 2 in the argument is that the mean temperature field is distorted by the convective term $\psi\theta$, in the heat equation; since both ψ and θ have components proportional to $\sin(\pi z)$, this will force a $\sin(2\pi z)$ dependence on the mean temperature. Similar remarks apply to the concentration field.

Taking the orthogonality condition with the eigen functions associated with the considered minimal model, we have:

$$\frac{dA_{11}(t)}{dt} = \frac{1}{\gamma_a \delta^2}\left[\alpha\, Rn\, C_{11}(t) - \alpha\, Ra\, B_{11}(t) - \nu\,\delta^2 A_{11}(t) - \nu\, C_P \delta^4 A_{11}(t)\right]$$

$$\frac{dB_{11}}{dt} = -\left[\alpha A_{11}(t) + \eta\delta^2 B_{11}(t) + \alpha\,\pi\, A_{11}(t)\, B_{02}(t)\right]$$

$$\frac{dB_{02}}{dt} = -\eta 4\pi^2 B_{02}(t) + \frac{\alpha\pi}{2} A_{11}(t) B_{11}(t)$$

$$\frac{dC_{11}}{dt} = -\sigma\left[\frac{1}{\varepsilon}\alpha A_{11}(t) + \delta^2\left(\frac{C_{11}(t)}{Ln} + \frac{N_A}{Ln} B_{11}(t)\right) + \frac{1}{\varepsilon}\alpha A_{11}(t) C_{02}(t)\right]$$

$$\frac{dC_{02}}{dt} = -\sigma\left[\frac{1}{Ln}4\pi^2 C_{02}(t) + 4\pi^2 B_{03}(t)\frac{N_A}{Ln} - \frac{a\pi}{2\varepsilon}A_{11}(t)C_{11}(t)\right] \quad (57a\text{-}e)$$

In the case of steady motion $\frac{d(\ )}{dt} = D_i = 0$, ($i$ = 1, 2, .., 5) and we write all D_i's in terms of A_{11}. Thus we get:

$$D_1 = \frac{1}{\gamma_a \delta^2}\left[\alpha\, Rn\, C_{11}(t) - \alpha\, Ra\, B_{11}(t) - \nu\,\delta^2 A_{11}(t) - \nu\, C_P \delta^4 A_{11}(t)\right]$$

$$D_2 = -[\alpha A_{11}(t) + \eta\delta^2 B_{11}(t) + \alpha\pi A_{11}(t) B_{02}(t)]$$

$$D_3 = -\eta 4\pi^2 B_{02}(t) + \frac{\alpha\pi}{2} A_{11}(t) B_{11}(t)$$

$$D_4 = -\sigma\left[\frac{1}{\varepsilon}\alpha\, A_{11}(t) + \delta^2\left[\frac{C_{11}(t)}{Ln} + \frac{N_A}{Ln} B_{11}(t)\right] + \frac{1}{\varepsilon}\alpha\, A_{11}(t)\, C_{02}(t)\right]$$

$$D_5 = -\sigma\left[\frac{1}{Ln}4\pi^2 C_{02}(t) + 4\pi^2 B_{02}(t)\frac{N_A}{Ln} - \frac{1}{\varepsilon}\frac{a\pi}{2}A_{11}(t)C_{11}(t)\right] \quad (58a\text{-}e)$$

and

$$D_1 = D_2 = D_3 = D_4 = D_5 = 0 \quad (59)$$

The above system of simultaneous autonomous ordinary differential equations is solved numerically using Runge–Kutta–Gill method. One may also conclude that the trajectories of the above equations will be confined to the finiteness of the ellipsoid. Thus, the effect of the parameters *Rn*, *Ln*, N_A on the trajectories is to attract them to a set of measure zero, or to a fixed point to say.

5. HEAT AND NANOPARTICLE TRANSPORT

The Nusselt number, *Nu* is defined as:

$$Nu(t) = \frac{\text{Heat transport by (conduction + convection)}}{\text{Heat transport by conduction}} = 1 + \left[\frac{\int_0^{2\pi}\frac{\partial T}{\partial z}\,dx}{\int_0^{2\pi/a}\frac{\partial T_B}{\partial z}\,dx}\right]_{z=0} \quad (60)$$

Substituting expressions (24) and (56) in above equation produces a simpler form for the time dependent Nusselt number given by:

$$Nu\ (t) = 1 - 2\pi B_{02}(t) \tag{60}$$

The time dependent Sherwood number (nanoparticle concentration version of Nusselt number), *Sh* is defined similar to the Nusselt number. Following the procedure adopted for arriving at *Nu(t)*, one can obtain the expression for *Sh(t)* in the form:

$$Sh(t) = \left(1 - 2\pi C_{02}(t)\right) + N_A\left(1 - 2\pi B_{02}(t)\right) \tag{61}$$

6. RESULTS AND DISCUSSION

The expressions of thermal Rayleigh number for stationary and oscillatory convections are given by Eqns. (46) and (50) respectively. **Figure 1a-d** shows the effect of various parameters on the neutral stability curves for stationary convection with variation in one of these parameters. The effect of nanoparticle concentration Rayleigh number *Rn* is shown in **Fig. 1a**. It is shown that the thermal Rayleigh number decreases with increase in nanoparticle concentration Rayleigh number *Rn*, which indicates that elevation in nanoparticle concentration Rayleigh number *Rn destabilizes* the system. It should be noted that the negative value of *Rn* indicates a *bottom-heavy* case (nanoparticles settling), while a positive value indicates a top-heavy case (nanoparticles rising). The effect of Lewis number *Ln* on the thermal Rayleigh number is shown in **Fig. 1b**. One can see that the thermal Rayleigh number increases with increase in Lewis number, indicating that the Lewis number has the opposite effect to nanoparticle concentration Rayleigh number *Rn* i.e. it *stabilizes* the system. The effect of viscosity ratio ν and thermal conductivity ratio η on the thermal Rayleigh number is depicted in **Figs. 1c and 1d** respectively, these figures show that as ν and η increases, Ra_T increases which indicates that both ν and η will stabilize the system. The effect of concentration Rayleigh number *Rn* and Lewis number *Ln* on thermal Rayleigh number Ra_T for stationary convection exhibits a similar pattern to the earlier results obtained by Long Sheu [63], although he employed an Oldroyd-B viscoelastic model which neglects

couple stress length effects. **Fig.1e** shows the effect of couple stress parameter. One can witness that the couple stress parameter enhances the stability of the system. In the absence of couple stress parameter C_P, all the results correspond to the Newtonian nanofluid results obtained by Umavathi and Mohite [64].

Figure 2a-g displays the variation of thermal Rayleigh number for oscillatory convection with respect to various parameters. In Fig. 2a it is seen that for negative values of *Rn* (bottom-heavy case) the thermal Rayleigh number decreases as *Rn* increases which will advance the onset of convection. As the Lewis number *Ln* increases the thermal Rayleigh number Ra_T decreases as seen in Fig. 2b which implies that Lewis number *Ln* destabilizes the system.

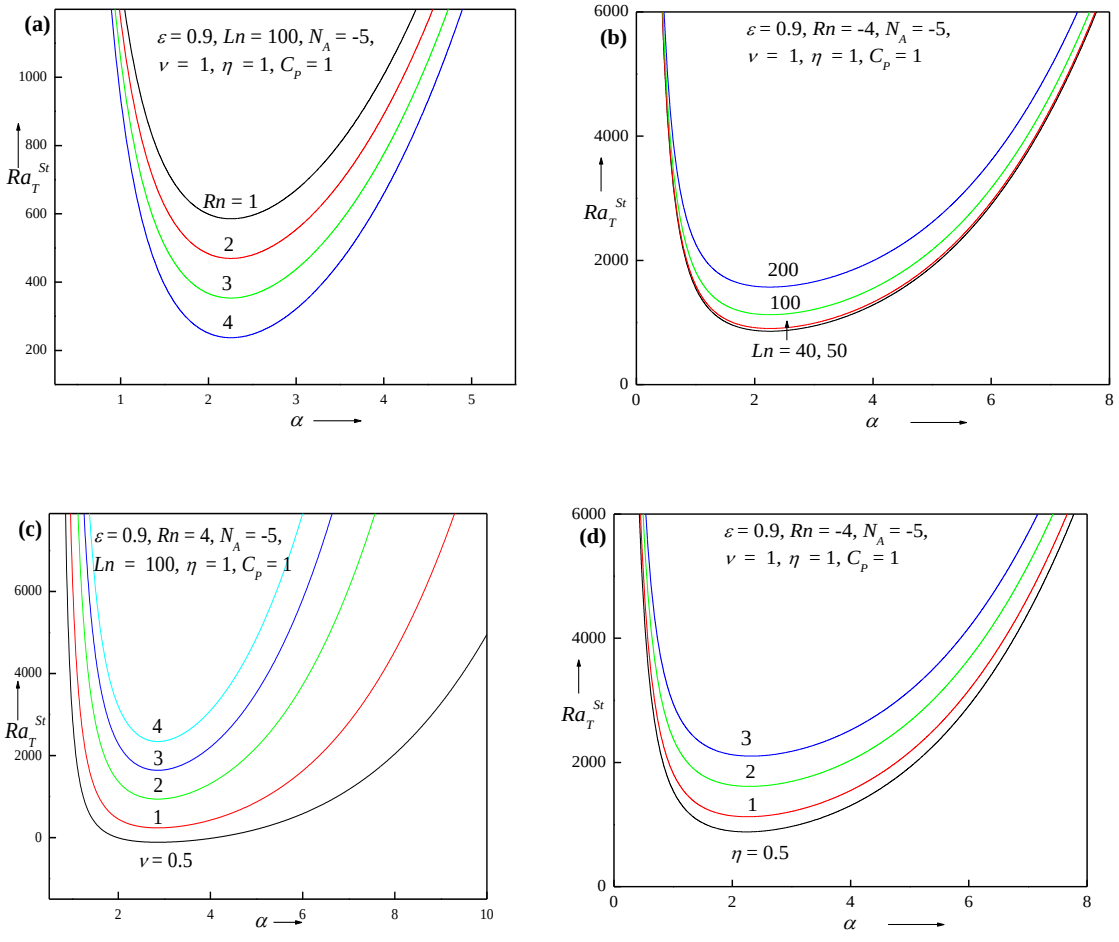

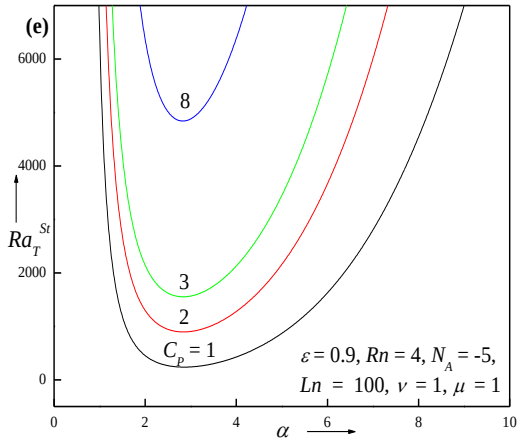

Fig. 1 Neutral curves on stationary convection for different values of **(a)** nanoparticle concentration Rayleigh number Rn, **(b)** Lewis number Ln, **(c)** Viscosity ratio ν, **(d)** conductivity ratio η, (e) couple stress parameter C_P.

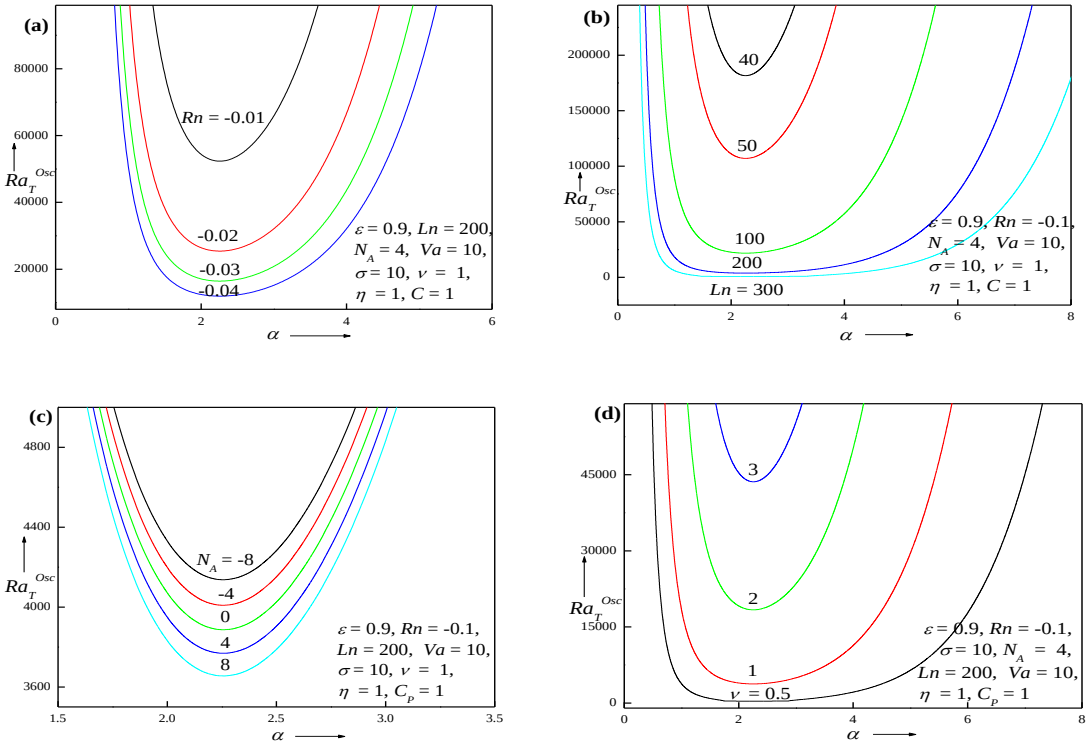

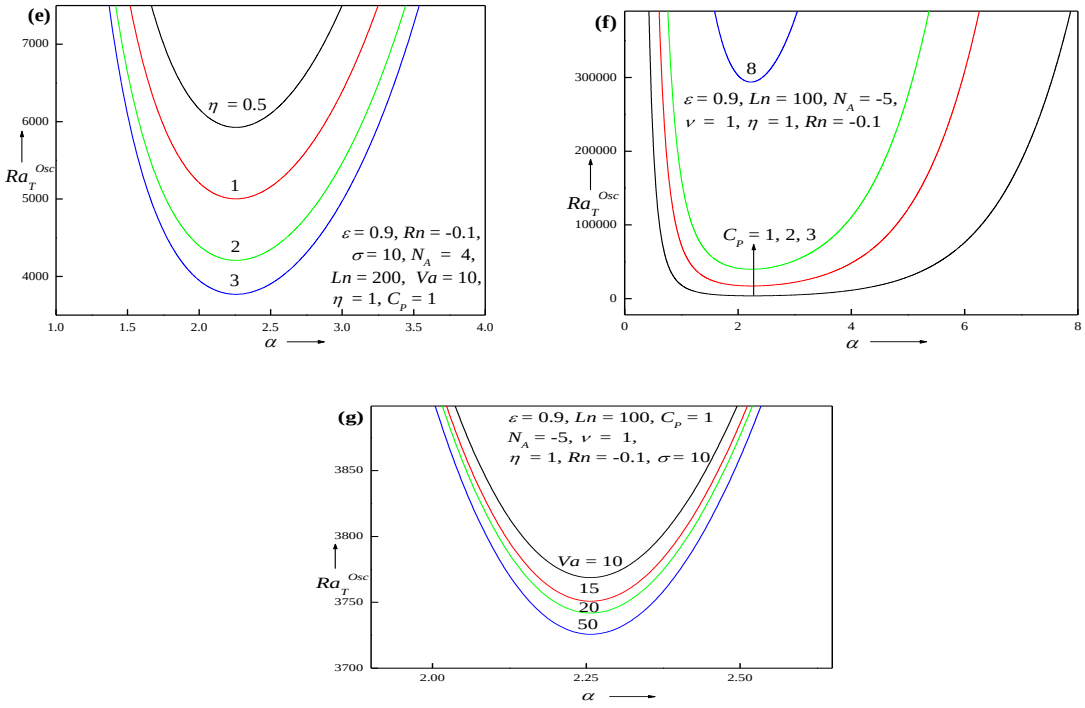

Fig. 2 Neutral curves on oscillatory convection for different values of **(a)** nanoparticle concentration Rayleigh number *Rn*, **(b)** Lewis number *Ln*, **(c)** modified diffusivity ratio N_A, **(d)** Viscosity ratio ν, **(e)** Thermal conductivity ratio η, **(f)** couple stress parameter C_P, **(g)** Vadász number *Va*.

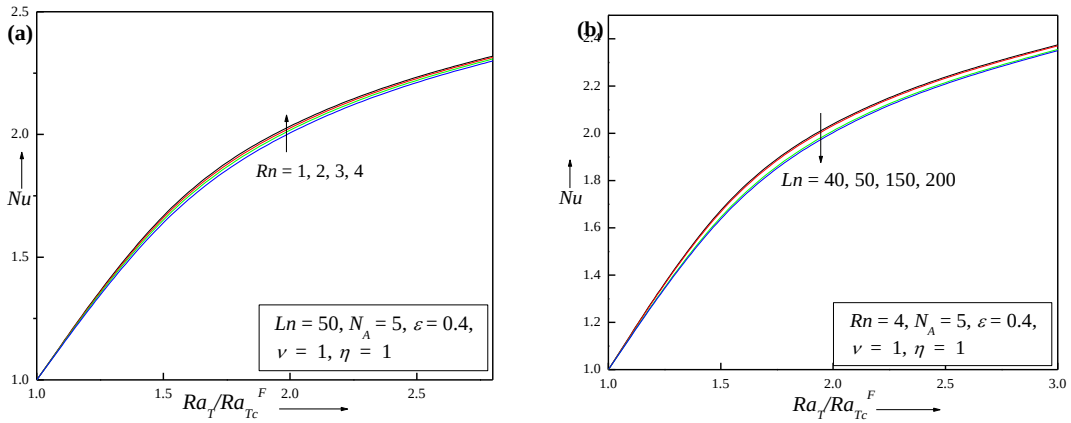

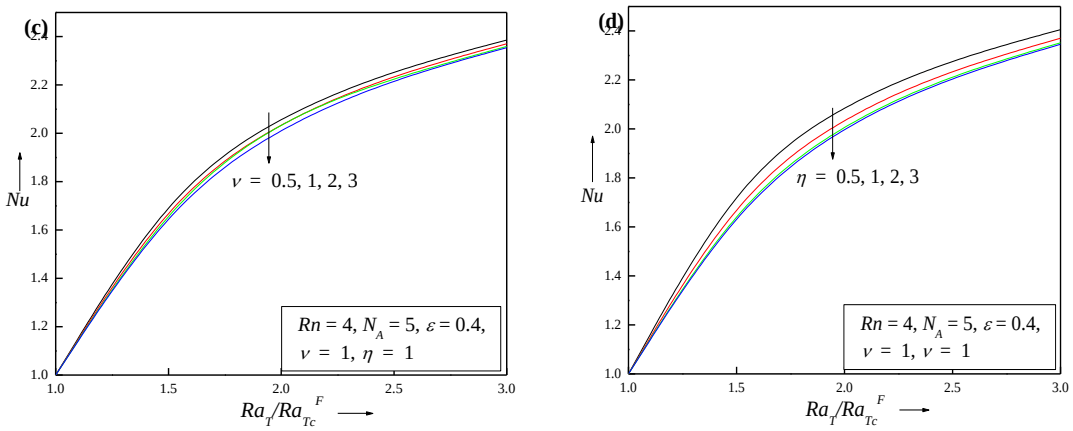

Fig. 3 Variation of Nusselt number *Nu* with critical Rayleigh Number for different values of **(a)** Nanoparticle concentration Rayleigh number *Rn*, **(b)** Lewis number *Ln*, **(c)** Viscosity ratio ν, **(d)** Thermal conductivity ratio η.

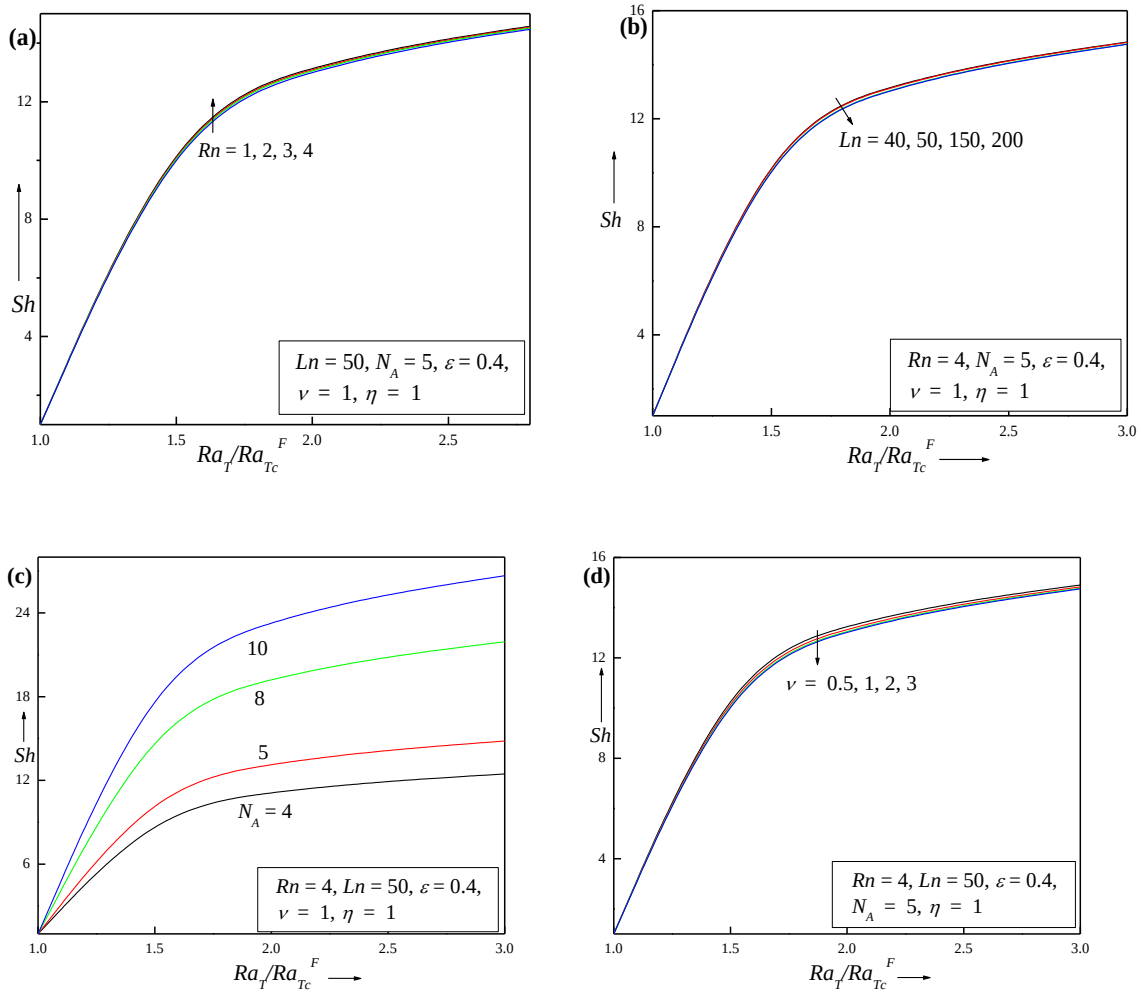

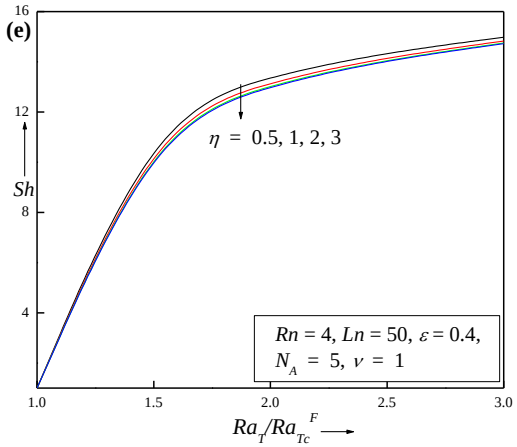

Fig. 4 Variation of Sherwood number *Sh* with critical Rayleigh Number for different values of **(a)** Nanoparticle concentration Rayleigh number *Rn*, **(b)** Lewis number *Ln*, **(c)** Modified diffusivity ratio N_A, **(d)** Viscosity ratio ν, **(e)** Thermal conductivity ratio η.

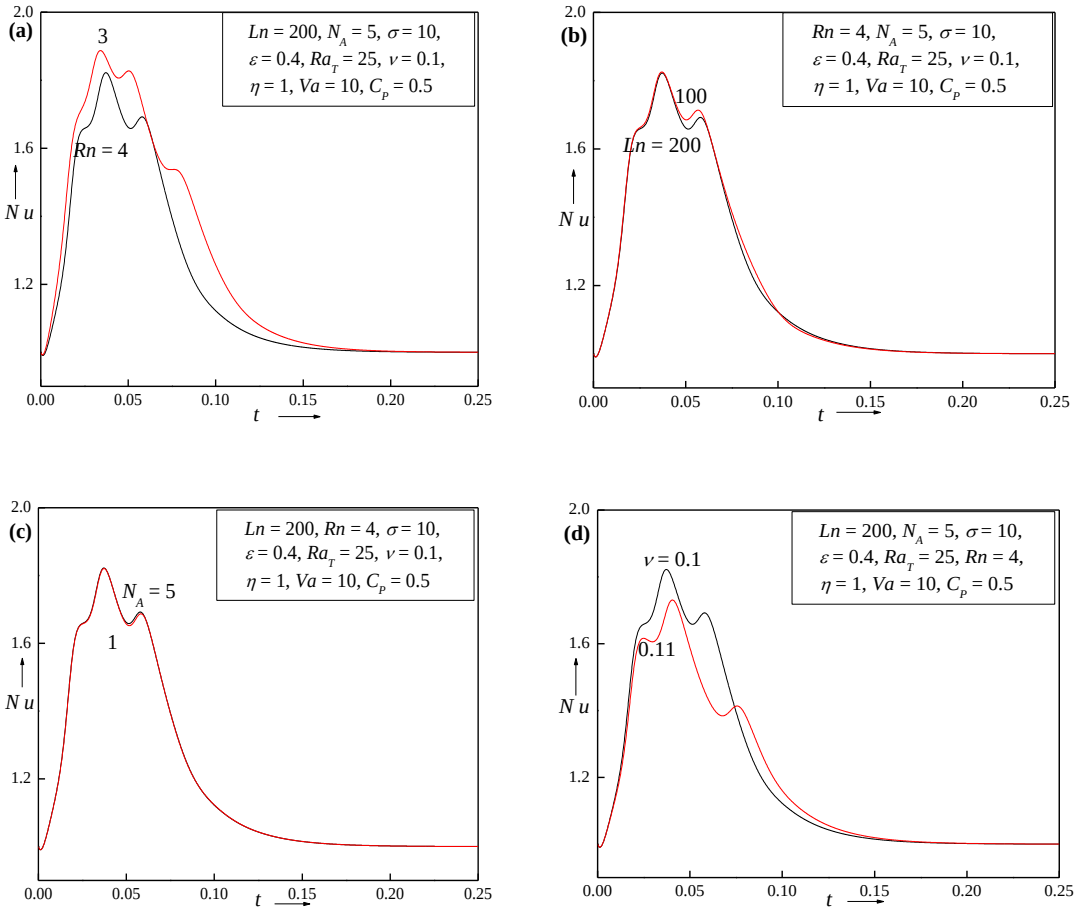

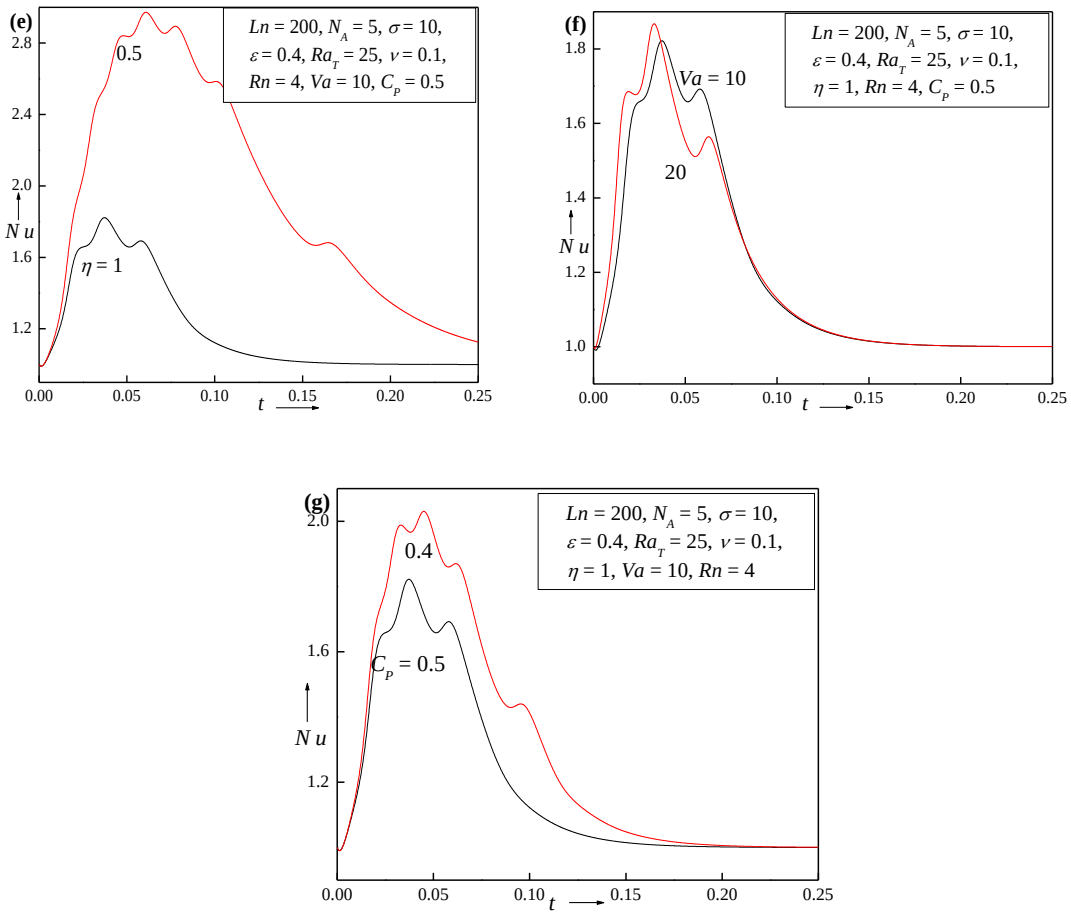

Fig. 5 Transient Nusselt number *Nu* with time for different values of **(a)** Nanoparticle concentration Rayleigh number *Rn*, **(b)** Lewis number *Ln*, **(c)** Modified diffusivity ratio N_A, **(d)** Viscosity ratio ν, **(e)** Thermal conductivity ratio η, **(f)** Vadász number *Va*, **(g)** couple stress parameter C_P.

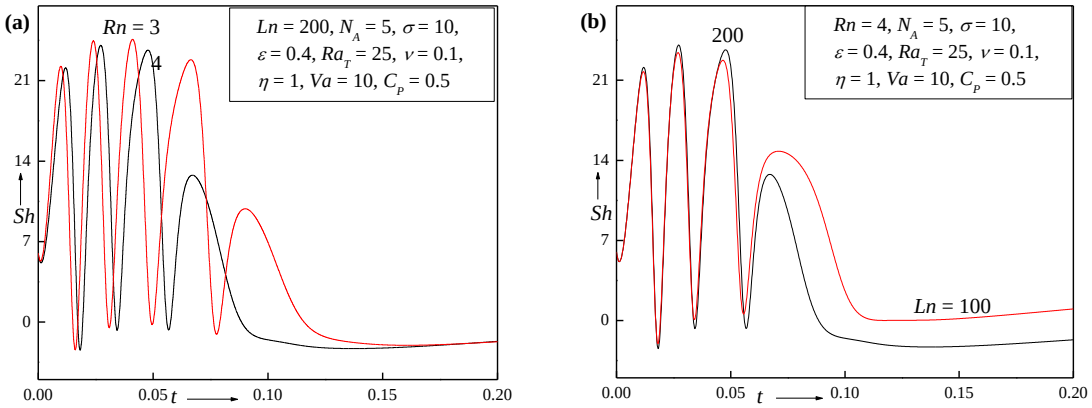

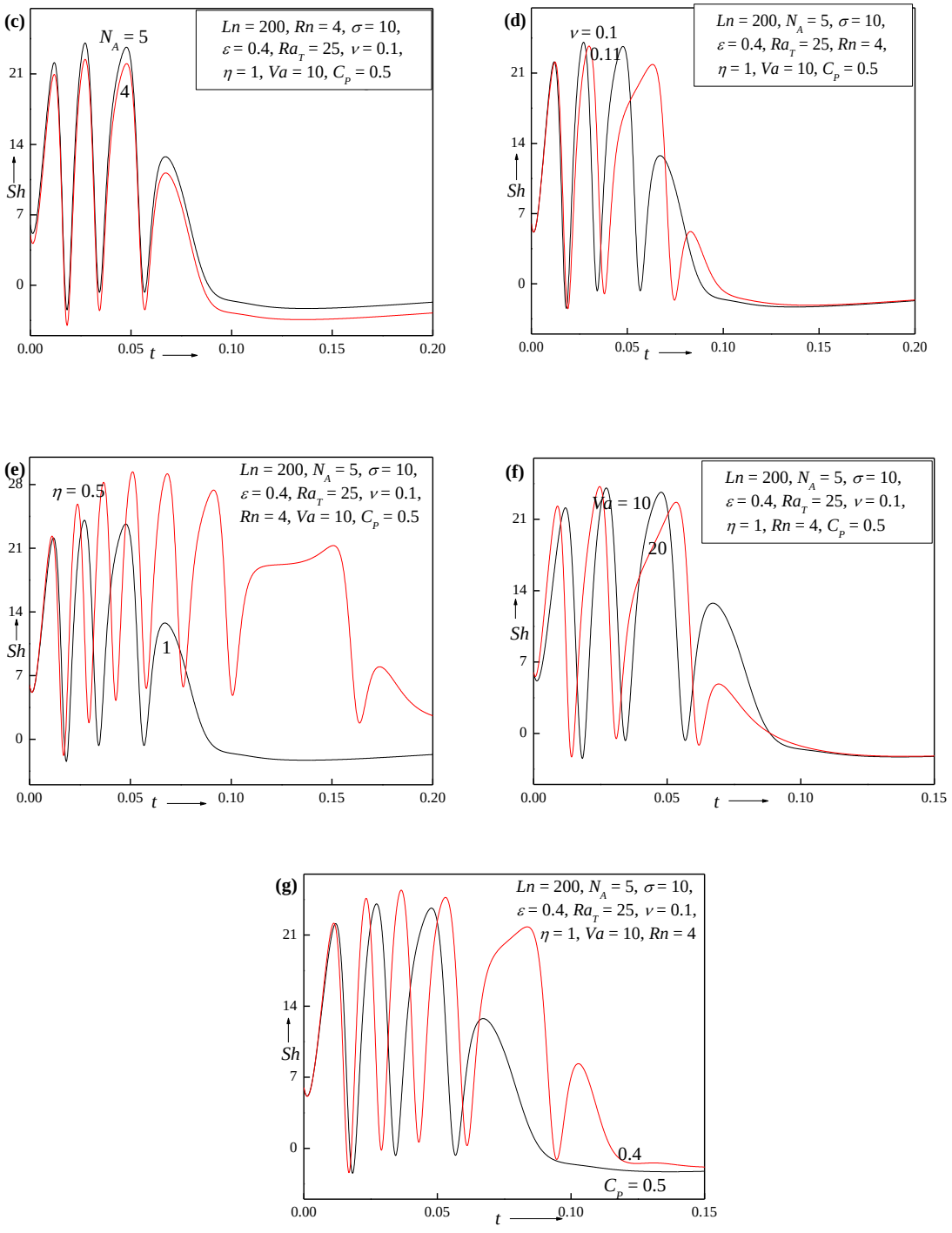

Fig. 6 Transient Sherwood number *Sh* with time for different values of **(a)** nanoparticle concentration Rayleigh number *Rn*, **(b)** Lewis number *Ln*, **(c)** modified diffusivity ratio N_A, **(d)** Viscosity ratio ν, **(e)** thermal conductivity ratio η, **(f)** Vadász number *Va*, **(g)** couple stress rheological parameter C_P.

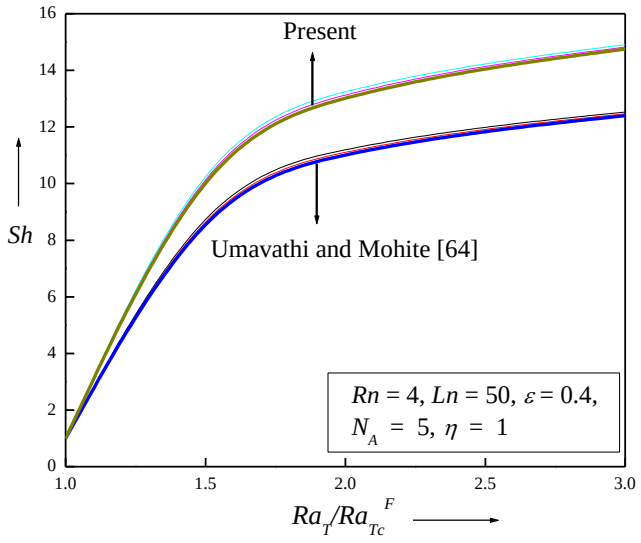

Fig. 7 Sherwood number *Sh* with critical Rayleigh Number for different values of viscosity ratio ν

The modified diffusivity ratio N_A decreases with the Rayleigh number, thus showing a destabilizing effect on the system (**Fig. 2c**). The effects of viscosity ratio ν and thermal conductivity ratio η on thermal Rayleigh number are depicted in **Figs. 2d and 2e** respectively. From these figures it is evident that enhancing ν increases the thermal Rayleigh number for oscillatory convection thus *delaying* the onset of convection; however elevation in η decreases the thermal Rayleigh number for oscillatory convection thus *advancing* the onset of convection. The effect of couple stress parameter C_P on thermal Rayleigh number is depicted in Fig. 2f. Inspection of the profiles indicates that as C_P increases the thermal Rayleigh number increases and therefore C_P stabilizes the system. Inspection of the definition of $C_P = \dfrac{\mu_C}{\mu_{eff} H^2}$ in Eqn. (12) and its eventual form in the double-diffusive modified momentum Eqn. (32) i.e. $\left(s\gamma_a + \tilde{\mu}(z) - \tilde{\mu}(z) Cp\nabla^2\right)\nabla^2 w' = Ra_T \nabla_H^2 T' - Rn\nabla_H^2 \phi'$ indicates that couple stress effect features as a quartic differential term CP∇4w in terms of the z-direction linear velocity component. Clearly C_P is quadratically inversely proportional to a length scale, *H*. Increasing C_P values are known to accelerate the flow with decreasing

length effect. This serves to contribute to a momentum modification which encourages a rise in thermal Rayleigh number. The effect of Vadász number *Va* on thermal Rayleigh number is depicted in Fig. 2g. From this figure one can see that as *Va* increases the thermal Rayleigh number decreases and thus larger values of *Va* destabilize the system. $Va = \frac{\varepsilon^2 \,\mathrm{Pr}}{Da}$ and therefore, increasing this parameter corresponds to greater medium porosity assuming *Pr* (ratio of momentum and thermal diffusivity) and *Da* (dimensionless scaled permeability) are fixed. The effect of concentration Rayleigh number *Rn* and Lewis number *Ln* on thermal Rayleigh number Ra_T for *oscillatory convection* also demonstrate similar results to those computed by Long Sheu [63]. The effect of increasing modified diffusivity ratio, N_A, couple stress parameter, C_P and Vadász number *Va* also produce trends similar (but not identical to) the results obtained by Malashetty *et al.* [65] (although in this study cross-diffusion effects and variable thermophysical properties were ignored).

The nonlinear analysis identifies not only the *onset threshold of finite amplitude motion* but also furnishes key details on heat and mass transport characteristics at the boundaries (microchannel plates) in terms of Nusselt *Nu* and Sherwood *Sh* numbers. *Nu* and *Sh* are computed as the functions of Ra_T, and the variations of these non-dimensional numbers with Ra_T for different parameter values are depicted in **Figs. 3a-d and 4a-e** respectively. It is apparent that in each case, Sherwood number is always greater than Nusselt number and both Nusselt number and Sherwood number start at the conduction state value 1 at the point of onset of steady finite amplitude convection. When Ra_T is increased beyond Ra_{Tc}, there is a sharp increase in the values of both *Nu* and *Sh*. However further increase in Ra_T will not change *Nu* and *Sh* significantly. It is to be noted that the upper bound of *Nu* is 3 (similar results were obtained by Malashetty *et al.* [66]). It should also be noted that the upper bound of *Sh* is *not 3* (similar results were obtained by Bhadauria and Agarwal [67]). The upper bound of *Nu* remains 3 only for both clear and nanofluid. However, the upper bound for *Sh* for clear fluid is 3 whereas *for nanofluid it is not fixed*. In Figs. 3a, 4a we observe that as the concentration Rayleigh number *Rn* increases, the value of *Nu* and *Sh* both increase thereby showing an increase in the *rate of heat and mass transport to the system boundaries (plates)*. Figures 3b and 4b shows that as Lewis number increases both *Nu* and *Sh* decreases, which

implies that increasing Lewis number (i.e. decreasing nanoparticle species diffusivity) suppresses the heat and mass transport to the boundaries. It is also evident that with elevation in modified diffusivity ratio N_A, there is no tangible effect induced on the Nusselt number distribution, whereas in Fig. 4c we observe that with increasing modified diffusivity ratio N_A the Sherwood number is noticeably accentuated (this trend is similar to the results reported in Bhadauria and Agarwal [67]. As the viscosity ratio ν (Figs. 3c and 4d) and thermal conductivity ratio η (Figs. 3d and 4e) increase, both *Nu* and *Sh* are depleted implying that ν and η suppresses the heat and mass transfer to the plates.

The linear solutions exhibit a considerable variety of behavior in the system, and the transition from linear to non-linear convection although relatively complicated provides a deeper insight into the thermo-solutal fluid dynamics of the regime. Time-dependent results needs to be scrutinized in order to analyze these mechanisms. The transition can be appreciated comprehensively by careful analysis of Eqn. (57), whose solution gives a detailed description of the *two-dimensional* problem. The autonomous system of unsteady finite amplitude equations is solved numerically using the Runge-Kutta method. The Nusselt and Sherwood numbers are evaluated as functions of time *t*; the unsteady transient behavior of *Nu* and *Sh* are visualized in Figs. 5a-f and 6a-f respectively. These figures indicate that initially i.e. when time is small, large scale oscillations are computed in the values of *Nu* and *Sh* indicating an unsteady rate of heat and mass transfer from the couple stress nanofluid to the boundaries. With subsequent elapse in time, these values approach the steady state corresponding to a near convection stage. Figure 5a depicts the transient nature of Nusselt number with variation in nanoparticle concentration Rayleigh number *Rn*. It is observed that as *Rn* increases *Nu* decreases, thus showing a substantial reduction in heat transfer to the boundaries, which corroborates the earlier simulations of Agarwal *et al.* [68]. From Figs. 5b, 5d, 5e and 5f we observe that as Lewis number, viscosity ratio, thermal conductivity ratio and Vadász number increase, *Nu decreases* indicating that there is *suppression in heat transfer to the walls* (and therefore heating within the sandwiched layer). The modified diffusivity ratio however enhances the heat transfer to the walls as seen in Fig. 5c and generates cooling in the sandwich layer. The couple stress parameter however suppresses the

heat transfer to the walls (i.e. exacerbates heating of the sandwich layer) and this pattern agrees with earlier computations by Malashetty *et al.* [65].

It is seen from Figs. 6a, 6d, 6e and 6f that as nanoparticle concentration Rayleigh number *Rn*, viscosity ratio ν, conductivity ratio η and Vadász number *Va* increases the Sherwood number (concentration Nusselt number) decreases, which implies there is a suppression of mass transport. The mass transport is enhanced for Lewis number *Ln* and modified diffusivity ratio N_A as seen in Fig. 6b and 6c respectively. The couple stress parameter suppresses the heat transport. Hence the heat and mass transport decreases with an increase in the values of couple stress parameter which is the similar result obtained by Malashetty *et al.* [65]. The implication is that non-Newtonian couple stress characteristics may be exploited to regulate markedly heat transfer in the regime and also to control the onset of oscillatory convection, which is not possible with Newtonian fluent media in microfluidics. Furthermore, couple stress fluids offer a different mechanism for influencing stationary and oscillatory convection modes as compared with other non-Newtonian nanofluids (e.g. viscoelastic). In the absence of couple stress parameter C_P, all the results for all the convection modes correspond to the *Newtonian nanofluid* results presented earlier by Umavathi and Mohite [64]. Figure 7 shows the plots of Sherwood number for variations of viscosity ratio ν obtained by Umavathi and Mohite [64] and the present work. Excellent correlation is achieved confirming the validity of the present computations.

7. CONCLUSIONS

A comprehensive study has been presented for both linear and non-linear stability analysis in a horizontal porous medium saturated by a couple stress rheological nanofluid, heated from below and cooled from above, using the Darcy model. The mathematical model derived features the effects of Brownian motion along with thermophoresis for nanoscale heat and mass transfer. Further the viscosity and thermal conductivity dependence on nanoparticle fraction have been addressed mathematically using the approach of Tiwari and Das [29]. Linear analysis has been performed using the established normal mode technique. However, for weakly nonlinear analysis, a truncated Fourier series representation having only two terms is utilized. The basic (fundamental) solution has been computed with a Galerkin weighted scheme. A detailed parametric study of the impact of key thermophysical

parameters on stationary and oscillatory convection modes has been conducted. Additionally, detailed computations have been performed for the influence of control parameters on the heat and mass transfer rates to the boundaries. The following conclusions may be drawn from the current investigation:

(i) For the *stationary* convection mode, increasing Lewis number *Ln*, viscosity ratio ν, thermal conductivity ratio η and couple stress rheological parameter C_P all have a stabilizing effect whereas greater nanoparticle concentration Rayleigh number *Rn* destabilizes the system.

(ii) For the *oscillatory* convection mode, enhancement in viscosity ratio ν and couple stress parameter C_P both serve to stabilize the system whereas elevation in nanoparticle concentration Rayleigh number *Rn*, Lewis number *Ln*, modified diffusivity ratio N_A, thermal conductivity ratio η, and Vadász number *Va* all act to destabilize the system.

(iii) Increasing couple stress non-Newtonian parameter C_P enhances the stability of the system for both the stationary and oscillatory convection modes.

(iv) For steady finite amplitude motions, the heat and mass transfer to the boundaries decreases with an increase in Lewis number *Ln*, viscosity ratio ν and thermal conductivity ratio η, whereas heat and mass transfer to the walls increases with higher values of nanoparticle concentration Rayleigh number *Rn*. The mass transfer rate increases with larger values of modified diffusivity ratio N_A and Vadász number *Va.*

(v) The transient Nusselt number and Sherwood numbers both increase with increase in Lewis number *Ln* and modified diffusivity ratio N_A whereas they are suppressed with greater nanoparticle concentration Rayleigh number *Rn*, viscosity ratio ν and thermal conductivity ratio η.

(vi) The heat and mass transfer rates to the boundaries both diminish with an increase in the value of couple stress parameter C_P.

(vii) The couple stress parameter C_P stabilizes the system for all convection modes and therefore promotes the onset of convection for all modes.

(viii)The evolutions in transient Nusselt number and Sherwood number are found to be oscillatory for small values of time, *t*; however, when *t* becomes very large both the transient Nusselt and Sherwood value approach their steady state values.

(viii) In the absence of couple stress parameter C_P, a*ll the results for all convection modes* reduce exactly to the Newtonian solutions obtained by Umavathi and Mohite [64].

The computation methods deployed in the present study have produced *stable and valid* solutions for both linear and nonlinear thermal instability. Future work may extend the analysis to *higher order corrections* to provide a deeper insight. The methodology described in the current paper may also be utilized to consider more complex *microstructural* fluids e.g. ferromagnetic [69] and biomagnetic micropolar fluids [70], which are also of relevance to modern micro/nanofluidics - efforts in all these directions are underway.

ACKNOWLEDGEMENTS

The authors are grateful to both reviewers for their comprehensive comments which have served to improve the present article.

REFERENCES

[1] K.M. Schultz and E.M. Furst (2011). High-throughput rheology in a microfluidic device**,** *Lab Chip*, 11, 3802-3809.

[2] Anna S.L. (2008) Non-Newtonian Fluids in Microfluidics. In: *Li D. (eds) Encyclopedia of Microfluidics and Nanofluidics*. Springer, Boston, MA.

[3] F. Tian *et al.* (2017). Microfluidic co-flow of Newtonian and viscoelastic fluids for high-resolution separation of microparticles, *Lab Chip*, 17, 3078-3085.

[4] X. Lu et al. (2017). Particle manipulations in non-Newtonian microfluidics: A review, *Journal of Colloid and Interface Science*, 500, 182-201.

[5] Galindo-Rosales FJ, Campo-Deano L, Pinho FT, van Bokhorst E, Hamersma PJ, Oliveira MSN, Alves MA (2012) Microfluidic systems for the analysis of viscoelastic fluid flow phenomena in porous media. *Microfluid. Nanofluid.*, 12:485–498.

[6] A. Karimi *et al*., Hydrodynamic mechanisms of cell and particle trapping in microfluidics, *Biomicrofluidics.* 2013 Mar; 7(2): 021501.

[7] Wong VL, Loizou K, Lau PL, Graham RS, Hewakandamby BN. (2017). Numerical studies of shear-thinning droplet formation in a microfluidic T-junction using two-phase level-set method. *Chemical Engineering Science*. 174:157-173.

[8] Choi SUS (1995) Enhancing thermal conductivity of fluids with nanoparticles. In: *Siginer, D.A.,Wang, H.P. (eds.) Development and Applications of Non-Newtonian Flows*, vols. MD-231, FED-66, ASME, New York, 99–105.

[9] Sireetorn Kuharat and O. Anwar Bég, Computational fluid dynamics simulation of a nanofluid-based annular solar collector with different metallic nanoparticles, *Heat and Mass Transfer Research Journal*, 3 (1), 1-23 (2019).
[10] Ankita Dubey, B. Vasu, O. Anwar Bég *and* Rama S R Gorla, Numerical simulation of two-fluid non-Newtonian nano-hemodynamics through a diseased artery with a stenosis and aneurysm, *Computer Methods in Biomechanics and Biomedical Engineering* (2020). **doi.org/10.1080/ 10255842.2020.1729755** (28 pages)
[11] O. Anwar Bég, S. Kuharat, M. Ferdows, M. Das, A. Kadir, M. Shamshuddin, Magnetic nano-polymer flow with magnetic induction and nanoparticle solid volume fraction effects: *solar magnetic nano-polymer fabrication simulation, Proc. IMechE-Part N: J Nanoengineering, Nanomaterials and Nano-systems (2019).* DOI: 10.1177/ 2397791419838714 (19 pages)
[12] O. Anwar Bég, Ayesha Sohail, T.A. Bég and A. Kadir, B-spline collocation simulation of nonlinear transient magnetic nano-bio-tribological squeeze film flow, *J. Mechanics in Medicine and Biology*, 18, 1850007.1- 1850007.20 (20 pages) (2018).
[13] O. Anwar Bég, D.E. Sanchez Espinoza, Ayesha Sohail, Ali Kadir, M. Shamshuddin, Experimental study of improved rheology and lubricity of drilling fluids enhanced with nanoparticles, *Applied Nanoscience*, 8,1069-1090 (2018).
[14] Das, S. K.; S. U. S. Choi; W. Yu; T. Pradeep, *Nanofluids: Science and Technology*. Wiley-Interscience, New York, USA (2007).
[15] Kumar S, Prasad SK, Banerjee J (2010) Analysis of flow and thermal field in nanofluid using a single-phase thermal dispersion model. *Appl. Math. Model*. 34:573–592.
[16] O. Anwar Bég, Nonlinear multi-physical laminar nanofluid bioconvection flows: Models and computation, *A. Sohail, Z. Li (Eds.): Computational Approaches in Biomedical Nano-Engineering, Wiley, Chapter 5, pp. 113-145 (2018).*
[17] P. Vadasz (2006). Heat conduction in nanofluid suspensions, *ASME J. Heat Transfer*. 128(5): 465-477.
[18] Gao L, Zhou XF (2006) Differential effective medium theory for thermal conductivity in nanofluids. *Phys. Lett. A*., 348(3–6):355–360.
[19] Gao L, Zhou X, Ding Y (2007) Effective thermal and electrical conductivity of carbon nanotube composites, *Chem. Phys. Lett*., 434 (4–6): 297–300.
[20] Zhou XF, Gao L (2006) Effective thermal conductivity in nanofluids of non-spherical particles with interfacial thermal resistance: differential effective medium theory, *J. Appl. Phys.*, 100(2):024913–024916.
[21] Keblinski P, Phillpot SR, Choi SUS, Eastman JA (2002) Mechanisms of heat flow in suspensions of nano-sized particles (nanofluids). *Int. J. Heat Mass Transfer*., 45(4): 855–863.
[22] Koo J, Kleinstreuer C (2005) Laminar nanofluid flow in microheat-sinks, *Int. J. Heat Mass Transfer.*, 48(13): 2652–2661.
[23] Karthikeyan NR, Philip J, Raj B (2008) Effect of clustering on the thermal conductivity of nanofluids, *Mater. Chem. Phys*., 109(1): 50–55.
[24] S. Chandrasekhar, *Hydrodynamic and Hydromagnetic Stability*, Oxford University Press, London (1968).
[25] Lapwood ER (1948) Convection of a fluid in a porous medium. *Proc. Cambridge Phil. Soc.* 44:508-521.
[26] B. Straughan (2014). Anisotropic inertia effect in microfluidic porous thermosolutal convection, *Microfluidics and Nanofluidics*, 16, 361–368.

[27] B. Anil *et al*., Heat transfer enhancement using non-Newtonian nanofluids in a shell and helical coil heat exchanger, *Experimental Thermal and Fluid Science*, 90, 132-142 (2018).
[28] A. Hussanan *et al.,* Convection heat transfer in micropolar nanofluids with oxide nanoparticles in water, kerosene and engine oil, *J. Molecular Liquids,* 229, 482-488 (2017).
[29] H. Chang *et al.* (2019). Rheological characteristics of non-Newtonian GPTMS-SiO_2 nanofluids, *International Communications in Heat and Mass Transfer,* 106, 38-45.
[30] S. Agarwal and P. Rana (2015). Thermal stability analysis of rotating porous layer with thermal non-equilibrium approach utilizing Al_2O_3–EG Oldroyd-B nanofluid, *Microfluidics and Nanofluidics,* 19, 117–131.
[31] J. Kang *et al.* (2014), Thermal instability of a nonhomogeneous power-law nanofluid in a porous layer with horizontal throughflow, *J. Non-Newtonian Fluid Mechanics,* 213, 50-56.
[32] Stokes, V. K. (1966) Couple stresses in fluids, *Phys. Fluids*, 9, 1709–1715.
[33] D'Ep, N. V. (1968). Equations of a fluid boundary layer with couple stresses. *Prikl. Math. Mech*.32, 748–753.
[34] Cowin S.C. (1974) The theory of polar fluids. *Adv. Appl. Mech.*, 14, 279-340.
[35] N. B. Naduvinamani and A Siddangouda (2007). Combined effects of surface roughness and couple stresses on squeeze film lubrication between porous circular stepped plates, *IMECHE: Journal of Engineering Tribology*, 221, 4.
[36] A. Raptis and H.S. Takhar (1999). Polar fluid through a porous medium, *Acta Mechanica* 135, 91–93 (1999).
[37] O. Anwar Bég, S.K. Ghosh, S. Ahmed and T. A. Bég, Mathematical modelling of oscillatory magneto-convection of a couple stress biofluid in an inclined rotating channel, *J. Mechanics Medicine and Biology*, 12, 3, 1250050-1 to 1250050-35 (2012).
[38] N.A. Khan *et al.* (2019)., Swirling flow of couple stress fluid due to a rotating disk, Nonlinear Engineering: *Modeling and Application,* 8: 261–269.
[39] J. V. Ramana Murthy, J. Srinivas and O. Anwar Bég, Entropy generation analysis of radiative heat transfer effects on channel flow of two immiscible couple stress fluids, *J. Brazilian Soc. Mech Sci. Eng,* 39, 2191–2202 (2017).
[40] N.A. Khan, F. Riaz, Off-centered stagnation point flow of a couple stress fluid towards a rotating disk, *The Sci. World J.*, 2014 (2014)163586.
[41] D. Tripathi, A. Yadav and O. Anwar Bég, Electro-osmotic flow of couple stress fluids in a micro-channel propagated by peristalsis, *European Physical Journal Plus,* 132: 173-185. (2017).
[42] T. Hayat, Z. Iqbal, M. Qasim, O.M. Aldossary, Heat transfer in a couple stress fluid over a continuous moving surface with internal heat generation and convective boundary conditions, *Zeitschrift für Naturforschung A: J. Physical Sciences,* 67a (2012) 217-224.
[43] H. Basha, G. Janardhana Reddy, N. S. Venkata Narayanan and O. Anwar Bég, Supercritical heat transfer characteristics of couple stress convection flow from a vertical cylinder using an equation of state approach, *J. Molecular Liquids* (2018). (20 pages) DOI.ORG/10.1016/J.MOLLIQ.2018.11.165
[44] Patil P.M. and Hiremath P.S. (1993): Free convection effects on the oscillatory flow of a couple stress fluid through a porous medium, *Acta Mechanica*, 98, 143.
[45] R. Nandal and A. Mahajan, (2018). Penetrative convection in couple-stress fluid via internal heat source/sink with the boundary effects, *J. Non-Newtonian Fluid Mechanics,* 260, 133-141.

[46] Sunil, D. R., A. Mahajan. Global stability for thermal convection in a couple-stress fluid. *International Communications in Heat and Mass Transfer*, 38 (2011) 938–942.
[47] S.B. N. Kumar *et al.* (2019). Exploration of Coriolis force on the linear stability of couple stress fluid flow induced by double diffusive convection, *ASME J. Heat Transfer*. 141(12): 122502 (11 pages).
[48] S.N. Gaikwad *et al.,* (2007). An analytical study of linear and non-linear double diffusive convection with Soret and Dufour effects in couple stress fluid, *International Journal of Non-Linear Mechanics,* 42, 903-913.
[49] Sharma RC, Thakur KD, Couple stress fluids heated from below in hydromagnetics, *Czech J. Phys*. 50 (6) 773-758. (2000).
[50] Sunil RC, Sharma RS, Chandel , On superposed couple-stress fluids in porous medium in hydromagnetics. *Z Naturforsch* 57a: 955–960 (2002).
[51] Sharma RC, Sharma M (2004) Effect of suspended particles on couple-stress fluid heated from below in the presence of rotation and magnetic field. *Indian J. Pure Appl. Math.* 35, 973–989 **(**2004).
[52] M.S. Malashetty *et al*., (2009). The onset of convection in a couple stress fluid saturated porous layer using a thermal non-equilibrium model, *Physics Letters A*, 373, 781-790.
[53] Buongiorno J. (2006) Convective transport in nanofluids. *ASME J. Heat Transfer*, 128:240–250.
[54] O. Anwar Bég and D. Tripathi, Peristaltic pumping of nanofluids, *Chapter 3, pages 69-96, Modeling and Simulation Methods and Applications, Eds (S. K. Basu, N. Kumar), Springer, Berlin, Germany* (2014).
[55] T. Hayat *et al*., (2017). On squeezed flow of couple stress nanofluid between two parallel plates, *Results in Physics*, 7, 553-561.
[56] S. Ghosh *et al*., Couple stress effects on three-dimensional flow of magnetite–water based nanofluid over an extended surface in presence of non-linear thermal radiation, *International Journal of Applied and Computational Mathematics,* 4, 11 (2018).
[57] Brinkman HC (1952) The viscosity of concentrated suspensions and solutions. *J. Chem. Physics.*, 20:571-581.
[58] Maxwell J.C. (1904) *A Treatise on Electricity and Magnetism*, 2nd edn. Oxford University Press, Cambridge.
[59] Nield DA (2008) General heterogeneity effects on the onset of convection in a porous medium. In: *Vadász, P. (ed.) Emerging topics in Heat and Mass Transfer in Porous Media,* pp. 63–84. Springer, New York.
[60] Kuznetsov AV, Nield DA (2010a). Thermal instability in a porous medium layer saturated by a nanofluids: Brinkman Model. *Transport in Porous Media*, 81:409-422.
[61] Kuznetsov AV, Nield DA (2010b). Effect of local thermal non-equilibrium on the onset of convection in porous medium layer saturated by a nanofluids. *Transport in Porous Media*, 83:425-436.
[62] Finlayson BA. (1972). *Method of Weighted Residual and Variational Principles*, Academic Press.
[63] L. J. Sheu (2011) Thermal instability in a porous medium layer saturated with a viscoelastic nanofluid, *Transp Porous Med*, 88: 461–477.
[64] J.C. Umavathi, Monica B. Mohite (2014) The onset of convection in a nanofluid saturated porous layer using Darcy model with cross diffusion. *Meccanica,* 49:1159–1175.

[65] Malashetty MS, Dual Pal, Premilla Kollur (2010) Double diffusive convection in a Darcy porous medium saturated with a couple-stress fluid, *Fluid Dyn. Res*. 42:035502 (21pp).
[66] Malashetty MS, Swamy MS, Sidram W (2011). Double diffusive convection in a rotating anisotropic porous layer saturated with viscoelastic fluid, *Int. J. Thermal Sciences*, 50 (9), 1757-1769.
[67] Bhadauria BS, Agarwal S (2011) Natural convection in a nanofluid saturated rotating porous layer: A nonlinear study. *Transp. Porous Media*., 87(2): 585–602.
[68] Agarwal S, Bhadauria BS, Sacheti NC, Chandran P, Singh AK (2012) Non-linear convective transport in a binary nanofluid saturated porous layer. *Transp. Porous Media*., 93:29–49.
[69] Rosensweig RE, (1985) *Ferrohydrodynamics*, Dover Reprints, New York, USA.
[70] Bég OA, Bhargava R, Rawat S, Takhar HS, Halim MK (2008). Computational modeling of biomagnetic micropolar blood flow and heat transfer in a two-dimensional non-Darcian porous medium, *Meccanica.,* 43, 4, 391-410.